UNIVERSIDAD DE CHILE
FACULTAD DE CIENCIAS FÍSICAS Y MATEMÁTICAS
DEPARTAMENTO DE INGENIERÍA MECÁNICA

RESIDUAL STRESS AND STRAIN MODELS IN PIPELINE WELDING, CONSIDERING MISALIGNED JOINTS.

MEMORIA PARA OPTAR AL TÍTULO DE INGENIERO CIVIL MECÁNICO

CÉSAR MAXIMILIANO GONZÁLEZ BISQUERTT

PROFESOR GUÍA:
PATRICIO MENDEZ PINTO

MIEMBROS DE LA COMISIÓN:
ROGER BUSTAMANTE PLAZA
RUBÉN FÉRNANDEZ URRUTIA

Este trabajo ha sido financiado parcialmente por:
Emerging Leaders in the Americas Program

SANTIAGO DE CHILE
2022

RESUMEN DE LA MEMORIA PARA OPTAR
AL TÍTULO DE INGENIERO CIVIL
POR: CÉSAR MAXIMILIANO GONZÁLEZ BISQUERTT
FECHA: 2022
PROFESOR GUIA: PATRICIO MENDEZ PINTO

MODELOS DE ESFUERZOS RESIDUALES Y DEFORMACIONES EN SOLDADURA DE TUBERÍAS, CONSIDERANDO UNIONES DESALINEADAS.

Este trabajo se centra en la predicción de esfuerzos residuales y distorsiones debidas a la soldadura de tuberías, la cual produce cierta cantidad de momento local a lo largo de la unión soldada. Bajo estas circunstancias, las discontinuidades en las uniones desalineadas afectan la susceptibilidad de falla de la tubería. La investigación consistió en exponer modelos que describen distorsiones, temperatura y tensiones residuales en soldadura, utilizar modelos rigurosos para calcular distorsiones y esfuerzos residuales en un caso de estudio de geometría cilíndrica y construir modelos computacionales para compararlos con las predicciones de la teoría.

Los resultados introducen modificaciones en los parámetros de las ecuaciones que describen el desplazamiento radial del perfil de la tubería permitiendo la disminución del error con respecto a los parámetros de la referencia. El cambio en los parámetros no proviene de un ajuste estadístico, sino que mediante el uso justificado de un campo de esfuerzos cilíndricos considerablemente diferente al de la referencia. Las ecuaciones que predicen los desplazamientos están listas para ser probados experimentalmente, donde resultados exitosos llevarían a la conclusión de que los esfuerzos residuales pronosticados también están bien planteados.

ABSTRACT
BY: CÉSAR MAXIMILIANO GONZÁLEZ BISQUERTT
DATE: 2022
THESIS ADVISOR: PATRICIO MENDEZ PINTO

RESIDUAL STRESS AND STRAIN MODELS IN PIPELINE WELDING, CONSIDERING MISALIGNED JOINTS.

This work is focused on predicting residual stresses and distortions in pipeline welding, which produces some amount of local bending across the weld joint. Under these circumstances, discontinuities in misaligned joints affect the pipeline's susceptibility to failure. The research consists of exposing models that describe distortions, temperature, and residual stresses in welding, revising rigorous models to calculate distortions and stresses in cylindrical geometries, and building computational models to compare them with predictions of the theory.

The results introduce modifications in the parameters on the equations that describe the radial displacement of the pipe profile with obtaining a decrease in the error concerning the reference parameters by using a considerably different stress field. The equations that predict displacements are ready to be tested experimentally, and successful results will lead to the conclusion that the predicted residual stresses are also well-posed.

To my parents César and Rocio

Acknowledgments

I would like to thank my advisor Professor Patricio F. Mendez, for his blind trust, patience, encouragement, and even the friendship he offered me during my internship at the University of Alberta. I will always appreciate all the opportunities he gave me.

Professor Roger Bustamante and Professor Rubén Férnandez for being members of my thesis committee, I deeply admire you.

I would also like to thank Mitchell, Goetz, for the selfless help that I receive from them and all the people that were working on the Canadian Center of Welding and Joining in 2021.

I'm also grateful with the good people and friends I meet during the career.

This research would not have been possible without the support of The Emerging Leaders in the Americas Program (ELAP) scholarships, And the license that Simufac provide to the laboratory

Table of Content

Table Index

Figure Index

Chapter 1

Introduction

1.1. Motivation

Distortion and residual stresses are recurring and costly problems resulting from welding. Both phenomena are produced as a result of the fast and restricted thermal expansion and shrinkage in the weld zone and surrounding material caused by the thermal action. [1]

Over the years, various models have attempted to predict welding distortions with greater precision. Currently, a revolutionary theory covering complex phenomena of plasticity in welding is being developed, this allows us to understand and predict distortions and residual stresses using rigorous but accessible parameters.

This work will be focused on the particular case of pipe line welding where the process results in residual tensile hoop stress which produces some amount of local bending across the weld joint. Under these circumstances, misaligned joints due to their non-ideal geometry have the potential to produce discontinuities and therefore affect the susceptibility to failure.[2]

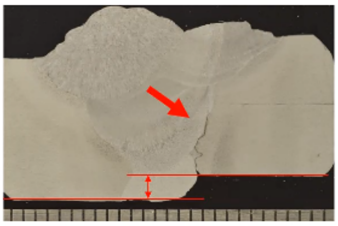

Figure 1.1: Cracking due to misalignmen

Thus arise the need to evaluate the functionality of the models by comparing their results with numerical simulations, using conditions present in procedures of the pipeline industry.

In the following pages, it is intended to explain in depth the methods used with their respective

assumptions, limitations, and scope. Therefore, this research involve concepts from different areas of engineering such as heat transfer, materials, mechanics, and computational methods.

1.2. Objectives

The goal of this work is to build computational models of the residual stresses and distortions of the welding process on pipeline joints and compare them with predictions of theoretical models. Contributing to the validation of the model, providing feedback and exploring its applications.

1.2.1. Specific objectives

- Generate a methodology to apply the theoretical model on study cases.
- Fix the parameters for admissible cases by the model and the simulation.
- Use Comsol and Simufact to simulate pipeline-welds with geometries and parameters of interest.
- Contrast the results with the theoretical model.
- Asses the results of numerical simulations in conjunction with theoretically calculated indexes.

1.3. Scopes

The work will consist mainly of comparing results of the theory of plasticity in welding with numerical simulations of distortions and residual stresses using the method of finite elements.

The parameters selected for the simulations come from procedures and dimensions used in the industry, where the assumptions from the model are applicable.

The case study include a:

- Methodology for its realization.
- Justification of the simplifications and the selected parameters.
- Numerical result of residual stresses and distortions obtained using FEM (finite element methods).
- Theoretically calculated values for residual stresses and distortions.
- Comparison between the results and the simulation.

Finally, the case study will be compared, quantifying the susceptibility to failure for different misalignment.

The ultimate goal of this work is to quantify the model accuracy through numerical validation and serve as feedback exploring its applications, and indirectly contributing to the design and execution of pipeline weld joints.

Chapter 2

Background

2.1. Weldment Distortions

Distortion in weldment results from non-uniform expansion and contraction in the filler metal and the metal adjacent to the weld, during heating and cooling cycle of the welding process. [3]

To understand how distortions occurs in thermal processes, it is useful to first consider the situation in Fig. 2.1. that shows the contrast between the uniformly heated bar that freely expands in all directions, then cools to room temperature contracting to its original dimensions, as shown in Fig. 2.1 (a) and the restrained bar where the expansion in one direction can not take place so when it contract uniformly the bar has been permanently distorted Fig 2.1 (b).

In a welded join the same kind of forces act between the weld metal and the base metal.

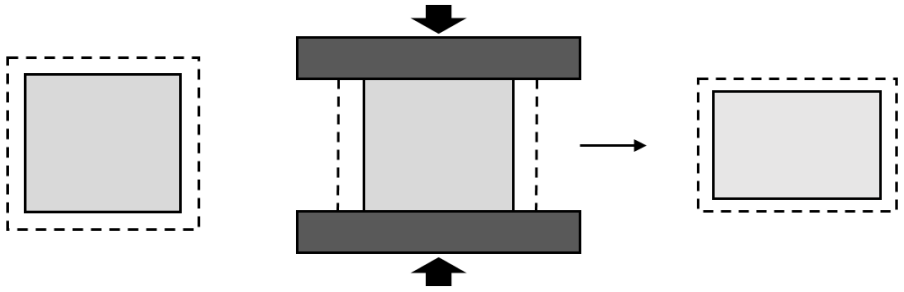

(a) Uniformly and unrestrained heated bar, at room temperature

(b) Restrained bar during heating and permanently deformed after cooling.

Figure 2.1: The thermal cycle of heating and cooling can cause permanent deformation when the free movement of the material is restricted.

In arc welding processes, the temperature varies radically with the distance from the heat source. By moving one millimeter, the peak temperatures can vary hundreds degrees K* see 2.5. Therefore the adjacent stiffer zones act by restricting the hotter zones in their expansion process, compressing

them during heating, and stretching them during cooling.This dispute between the different thermal deformations in the merged metal generates plastic deformations.

2.1.1. Factors Affecting distortion

Welding involves a large number of differing and interacting factors which affect the type and extent of distortion produced in a weldment, some examples are listed bellow [1]:

- The previous stresses in the material.
- The amount and type of restraint.
- Mechanical and thermal properties of the base metal.
- The joint design.
- The welding procedure.

2.1.2. Types of distortions

Butt welding is generally used in pipeline joins. The different types of distortions distinguished in these welds are; (a) longitudinal shrinkage, (b) transverse shrinkage, and (c) angular distortions. These are shown in Fig.2.2

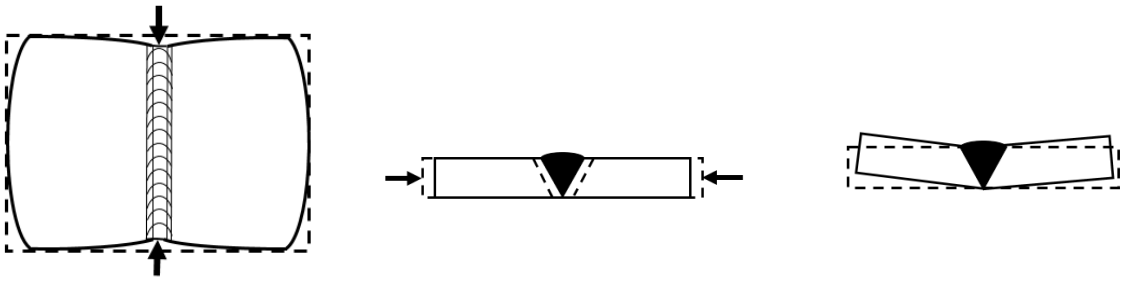

(a) Longitudinal Shrinkage. (b) Transverse shrinkage. (c) Angular distortions.

Figure 2.2: Types of distortions

In practice this types of distortions and the residual stresses that they rise act simultaneously interacting with each other and thus generating more complex distortion patterns. Nevertheless is the longitudinal shrinkage the cause of the tensile hoop stress in pipeline welding and the subject that will be treated separately in this work.

2.2. Temperature

The most fundamental aspect in fusion welding, is that just a part of the base metal is molten and, the rest remains solid. Thus fusion welding is a non-equilibrium process with a temperature gradient that allows this process to happen. This temperature gradient is also the cause of distortions and residual stresses.

Physical and mechanical properties change as heat is applied since they depend on temperature, therefore a description of the heat transfer on the model is needed to characterize the material and its behavior during the process (as any other thermodynamic system). Fig. 2.3 includes the evolution of yield strength, modulus of elasticity and coefficient of thermal expansion as a function of temperature. The temperature dependence of all these properties complicate precise calculations in weldment distortion.

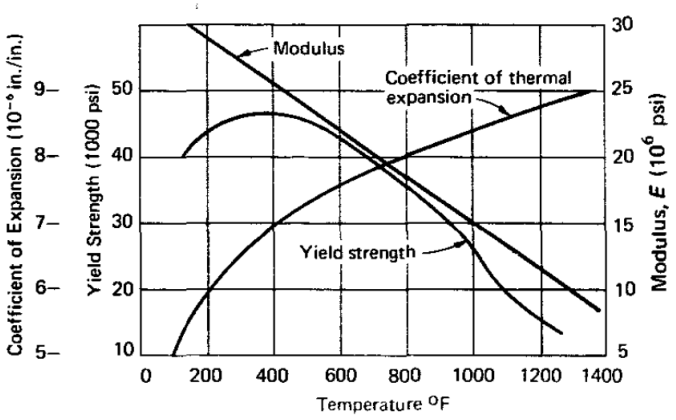

Figure 2.3: Changes in the properties of steel with increases in temperature.[3]

Temperature not only determines the dynamics of the process, but also the temperature History will leave its mark on the material. That is the case of distortions and residual stresses. It is essential, therefore, to know the temperature distribution and it evolution in time.

Most pipeline welding processes involve arc welding. Arc welding can be represented as a moving heat sources. The heat transfer theory due to a moving point source was first applied to arc welding by Rosenthal using the experimentally established principle of a "quasi-stationary state". [1] The model is a minimal representation of moving heat sources where the torch moves in straight line at constant velocity, the plate has infinite length and width, and thermophysical properties are considered constant.

Some of the following nomenclature will be used in this section:

[1] If the solid is large enough compared to the extent of heat, the temperature distribution around the heat source soon becomes constant. This state is called quasi-stationary and is defined by Equation (2.3) [4]

Table 2.1: Temperature section nomenclature

Variable	Unit	Description
T	K	Temperature
t	s	Time
x,y,z	m	Cartesian coordinates
q	W	Power absorbed by the substrate
α	m^2/s	Thermal diffusivity
k	$W/(mK)$	Heat conductivity
d	m	Thickness of the plate
U	m/s	Speed of the moving heat source
Q'	J/m	Linear heat input
h	$W/(m^2K)$	Convection coefficient on top surface
h'	$W/(m^2K)$	Convection coefficient on bottom surface
E	N/m^2	Young Modulus
ρ	Kg/m^3	Density
c	J/K	Heat Capacity

The governing equation is:

$$\frac{\partial^2 T}{\partial x^2}+\frac{\partial^2 T}{\partial y^2}+\frac{\partial^2 T}{\partial z^2}=\frac{1}{\alpha}\frac{\partial T}{\partial t} \tag{2.1}$$

When making the variable change of $\xi = x - Ut$,where ξ is the horizontal distance to the heat source. There follows:

$$\frac{\partial^2 T}{\partial \xi^2}+\frac{\partial^2 T}{\partial y^2}+\frac{\partial^2 T}{\partial z^2}=-\frac{U}{\alpha}\frac{\partial T}{\partial \xi}+\frac{1}{\alpha}\frac{\partial T}{\partial t} \tag{2.2}$$

Now been quasi-stationary means that $\frac{\partial T}{\partial t}=0$

$$\frac{\partial^2 T}{\partial \xi^2}+\frac{\partial^2 T}{\partial y^2}+\frac{\partial^2 T}{\partial z^2}=-\frac{U}{\alpha}\frac{\partial T}{\partial \xi} \tag{2.3}$$

Although there are 3d solutions used in thick plates, this work will consider the situation represented in Fig 2.4 and eq. (2.4) that approximates the situation in thin plates where it can be assumed $\frac{\partial T}{\partial dz}=0$ i.e there are no temperature gradient through the thickness.

The coordinates of eq. (2.2) are called Eulerian coordinates. The Eulerian coordinates x and y

that will be used from now on are defined in Fig. 2.4 letting ξ be call x.

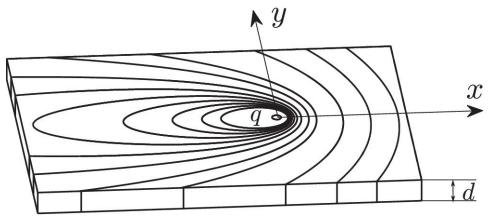

Figure 2.4: Isotherms for a 2-D point heat source of intensity q on a substrate of thickness d. [5]

Also surface heat losses by convection can be taken into account adding the term $\frac{h+h'}{kd}(T-T_0)$ obtaining:

$$\frac{\partial^2 T}{\partial x^2}+\frac{\partial^2 T}{\partial y^2}=-\frac{U}{\alpha}\frac{\partial T}{\partial x}+\frac{h+h'}{kd}(T-T_0)^2 \tag{2.4}$$

With boundary conditions:

$$\lim_{r\to 0}\frac{\partial T}{\partial r}=-\frac{q}{2\pi rkd} \tag{2.5}$$

$$\lim_{r\to\infty} T=T_0 \tag{2.6}$$

Where $r=\sqrt{x^2+y^2}$ is the distance from the moving source.

The first boundary condition comes from assuming the heat source 'q' is concentrated in an infinitesimal area.

The second comes from assuming that the base metal is infinitely large with respect to thermal input.

Equation (2.4) was solved by Rosenthal in [4]. This review comes from [5] giving an expression for temperature field:

$$T(x,y)=T_0+\frac{q}{2\pi rkd}\exp\left(-\frac{Ux}{2\alpha}\right)K_0(r\sqrt{\frac{U}{2\alpha}^2+\frac{h+h'}{kd}}) \tag{2.7}$$

Where K_0 is the modified Bessel function of second kind and zero order.

[2] Selecting the origin of the reference system in the heat source, ξ can now be called x.

In figure 2.5 there is an example of the solution of this equation with the properties of 1018 steel.

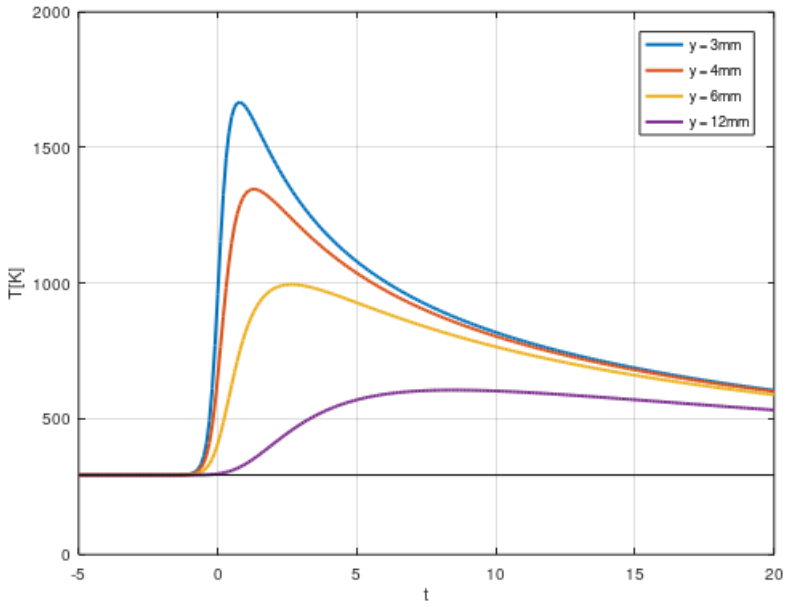

Figure 2.5: Solutions for (2.7) using q = 6000W, U = 6.16mm/s for 1cm thick plate of 1018 steel

In figure 2.5 it stand out that at small increases in distance the maximum temperature reached decreases considerably.

Maximum isotherm width

Although the solution (2.7) cannot be analytically inverted, the work exposed in [5] provides relatively simple expressions for the value y_{max} that represents the with of the zone that reaches or exceeds a given temperature. With these expressions, It is possible to calculate the size of zones differently affected by the temperature.

The isotherm half-width (Y_{max}) of a given temperature (T_{max}) for a fast moving heat source in a thin plate, with negligible heat losses is given by the asymptotic Rosenthal equation [4]:

$$y_{max}|_T = \frac{1}{\sqrt{2\pi e}} \frac{Q'}{d\rho c} \frac{1}{\Delta T_{max}} \tag{2.8}$$

2.3. Residual stresses

Residual stresses are stresses that remain after the original cause of the stresses has been removed. Residual stresses can result from thermal cycles and phase transformations during welding.

Due to the high-temperature gradients in welding, the thermal deformations aren't uniform. In these cases, the substrate it's not deforming just by thermal expansion but also suffers plastic and elastic strain to maintain its continuity. Later, when the substrate goes back to room temperature, thermal strain vanishes but plastic and elastic strains remain. This remaining elastic strain causes the permanence of stress.

To model residual stresses related to longitudinal shrinkage, a beginning is to idealize a weldment between two plates using the three-bar model shown in Fig 2.6. The middle bar represents the plasticity zone, which is the region where the thermal strain exceeds the elastic strain limit of the material i.e. yielding strain. The other two cylinders represent the rest of the material that didn't suffer plastic strains due to temperature changes.

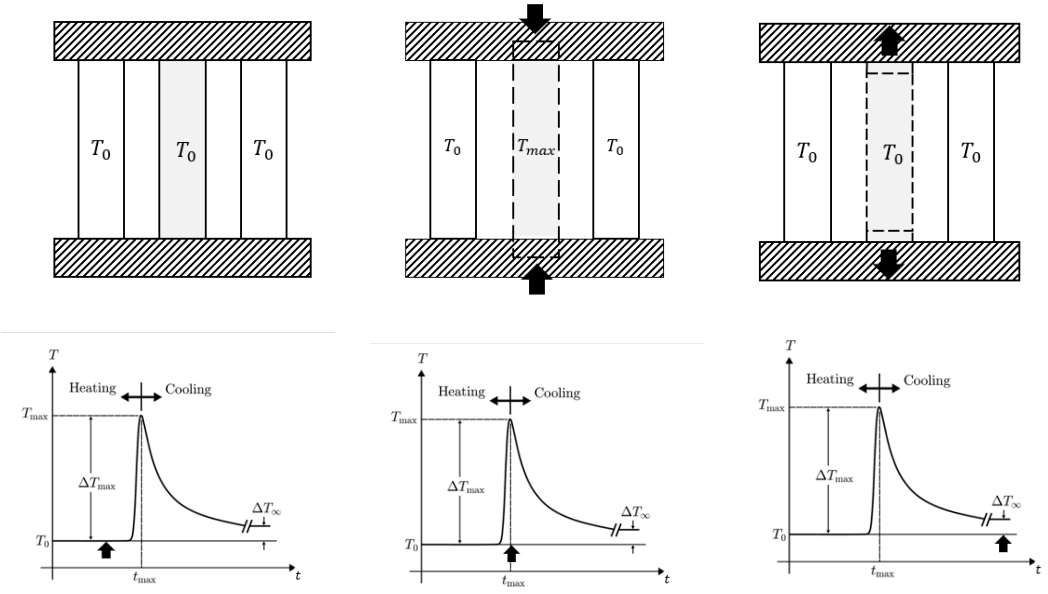

(a) Initial situation at room temperature T_0, stress-free

(b) At peak temperature, The middle bar reaches its maximal plastic strain

(c) At the end of the process the unstressed length of the middle bar it's shorter than the others so there is a remaining elastic strain and stress.

Figure 2.6: Three bar model.

These three bars are constricted to have the same length since all represent a single body so, the total strain is the same in the three bars. This situation generates plastic and elastic strain so the three bars can have equal size during the thermal cycle.

Similar to what happens in figure 2.1 after the thermal cycle, the dimensions of the middle bar change permanently, in this case becoming shorter. At equilibrium temperature, there is no more thermal strain. Thus all the bars present residual elastic strain to offset their different unstressed sizes.

In the three-bar model, the residual stress in the middle bar is tensile, and due to the equilibrium condition, the other two cylinders are under compressive stress.

In reality, the situation does not consist of three equal cylinders. It is a continuous plate instead. Typically the area that doesn't suffer plastic deformation is large compared to the plastic-affected zone. One can think that the region far from the heat source has a low and uniform reaction strain distributed along with the plate, and the smaller region near the heat source presents a higher residual elastic strain. The stress distribution has the shape of the referential Fig. 2.7.

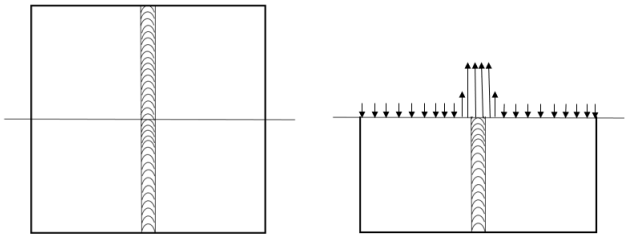

Figure 2.7: Residual stress distribution shape across the plate

2.3.1. Strain in thermal processes

The relationship between temperature and elastic strain is the key to calculating residual stress. In practical applications to material characterization, the elastic strain and thermal strain are typically inferred from direct measurement of force and temperature in a restricted bar during a thermal cycle. Satoh [27] first presented a suitable experimental apparatus and thus the force-temperature diagram is commonly associated with the "Satoh Test". [6]

Describing the Satoh test in different thermal cycles will allow inferring the plastic strain as a function of the maximum temperature reached.

Table 2.2 defines types of strain required in this work.[3]

[3] In the framework of longitudinal shrinkage is enough to consider the component of the strain parallel to the heat source trajectory. This is equivalent to just consider ε_{xx} in the coordinate system of Fig. 2.4

Table 2.2: Strain nomenclature

Variable	Description
ε_{th}	Thermal strain, caused by thermal expansion $\varepsilon_{th} = \alpha\Delta T$
ε_{el}	Elastic strain, Is the component that complies $\varepsilon_{el} = E\sigma$ at any point of the cycle.
ε_{pl}	Plastic strain, the permanent strain generated after yielding
ε_T	Total strain distribution, in general $\varepsilon_T = \varepsilon_{el} + \varepsilon_{pl} + \varepsilon_{th}$[a]
ε_{res}	Is the residual elastic strain distribution in the material (strains that could be measured).
ε_Y	The strain at yielding stress $\varepsilon_Y = \sigma_Y / E$
ε_{rxn}	Reaction strain fictitious strain distribution caused by the tendon force
ε_{inh}	Inherent strain $\varepsilon_{inh} \equiv \varepsilon_{res} - \varepsilon_{rxn}$

[a] This assumption is valid when the strains are small

From here the work will only consider very large or very rigid geometries, where the magnitude of the total strain of the assemble can be neglected like in a rigidly constrained specimen ($\varepsilon_T = 0$) i.e. the sum of the thermal, elastic, and plastic strains will always be zero. This means that the plastic strain can be obtained from the difference of the thermal and elastic strain.

The following description of figure 2.8 and its implications are directly extracted from [6]

" *Fig. 2.8 shows a typical diagram of elastic strain (force) vs. thermal strain (temperature) that displays three different thermal cycles with maximum temperatures corresponding to points a', b and b'.*

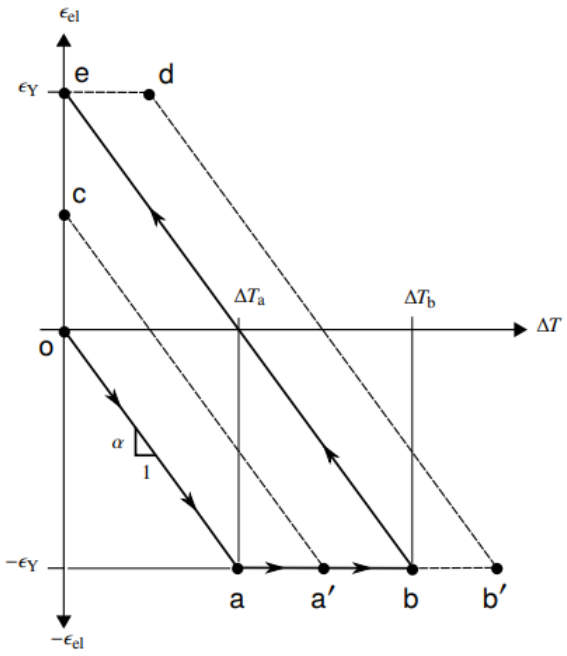

Figure 2.8: Relationship between elastic strain and temperature for thermal cycles with three different maximum temperatures [6]

The cycle with the lowest maximum temperature is o - a - a'-c. From point "o" to point "a" the bar thermally expands and elastically compress up to the critical point "a" where it reaches yielding at temperature T_a defined as the "first yield temperature" T_{Y1} can be calculated according to (2.9):

$$\Delta T_{Y1} = \frac{\varepsilon_Y}{\alpha} \tag{2.9}$$

From point a to point a', the thermal strain is further increased resulting in the development of a compressive (negative) plastic strain $\varepsilon_{pl} = \varepsilon_{th}|_{\Delta T_a} - \varepsilon_{th}|_{\Delta T_{a'}}$.

At point a', the temperature and thermal strain reach their maximum value. From point a' to point c, the thermal strain decreases, the elastic strain increases proportionally and the plastic strain remains unchanged. The residual plastic strain at point c is therefore equal to the plastic strain at point a'. The residual elastic strain at point c is positive (tensile) with a magnitude less than the yield strain (ε_Y*).*

The cycle with the intermediate maximum temperature is o - a -b - e. From point o to point a', the material behavior is identical to the previous cycle. From point a' to point b, additional compressive (negative) plastic strain develops to a maximum value of
$\varepsilon_{pl} = \varepsilon_{th}|_{\Delta T_{a'}} - \varepsilon_{th}|_{\Delta T_b}$ *at point b. From point b to point e, the thermal strain decreases and the*

elastic strain increases proportionally while the plastic strain remains constant. The plastic strain at point e is therefore equal to the plastic strain at point b. This cycle is unique in that the residual elastic strain at point e is equal to the yield strain (ε_Y). Since in the final state the thermal strain is also equal to zero, it follows that the residual plastic strain is equal and opposite to the residual elastic strain. The maximum temperature for this cycle at point b marks the minimum temperature change necessary to produce yield magnitude residual plastic strain during cooling.

This critical temperature is defined as the "second yield temperature," and for constant material properties is given by:

$$\Delta T_{Y2} = 2\frac{\varepsilon_Y}{\alpha} \tag{2.10}$$

The cycle with the highest maximum temperature is o - a - b' - d - e. From point o to point b, the material behavior is identical to the previous cycle. From point b to point b', additional compressive (negative) plastic strain develops to a maximum value of $\varepsilon_{pl} = \varepsilon_{th}|_{\Delta T_{b'}} - \varepsilon_{th}|_{\Delta T_a}$ at point b'. From point b' to point d the temperature and thermal strain decrease, the elastic strain increases proportionally and the plastic strain remains constant. At point d, the material begins to yield in tension and develop tensile (positive) plastic strain. From point d to point e, the thermal strain decreases back to zero as the temperature returns to ambient. At point e the thermal strain is zero and the residual elastic strain is equal to ε_Y. The residual plastic strain will therefore also have a magnitude equal to the yield strain. This result is verified by observing that the tensile plastic strain developed between point d and point e is equal and opposite to the compressive (negative) plastic strain developed between point b and point b'."

The function from (2.11) summarize the explanation above, giving the remaining plastic strain as a function of the maximum temperature reached:

$$\varepsilon_{pl}(T_{max}) = \begin{cases} 0, & T_{max} < T_{Y1} \\ \alpha(T_{Y1} - T_{max}), & T_{Y1} \leq T_{max} < T_{Y2} \\ \alpha(T_{Y1} - T_{Y2}) = -\varepsilon_y, & T_{max} > T_{Y2} \end{cases} \tag{2.11}$$

2.3.2. Tendon force

When it comes to longitudinal residual stresses, it is observed that the effect of the weld bead on a plate is similar to that of a force applied longitudinally in the direction of the weld, as indicated by the analogy of the Lincoln Procedure Hand-book in Fig. 2.9.

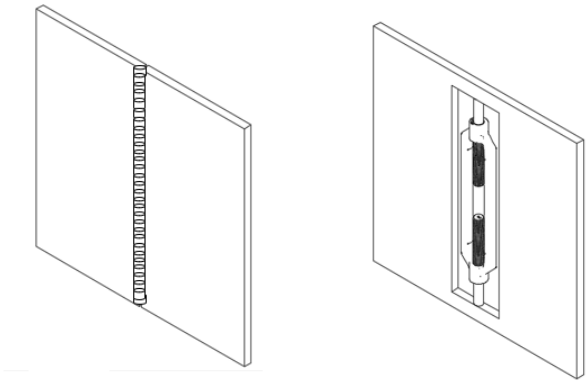

(a) Shrinkage in a centerline weld

(b) Similar effect as if the plate had a turnbuckle shorten the center line

Figure 2.9: Turnbuckle analogy

The concept of tendon force comes to represent this effect as if longitudinal external load was acting upon the plate. This is not a bad approximation because except for a relatively small area where reached temperatures generates plastic deformations, the residual strain (and consequently stress) along the plate is uniform and corresponds to the plate reaction to the large stresses in the plasticity zone.

This is how ε_{rxn} strain from Fig. 2.10.a is defined in [6].

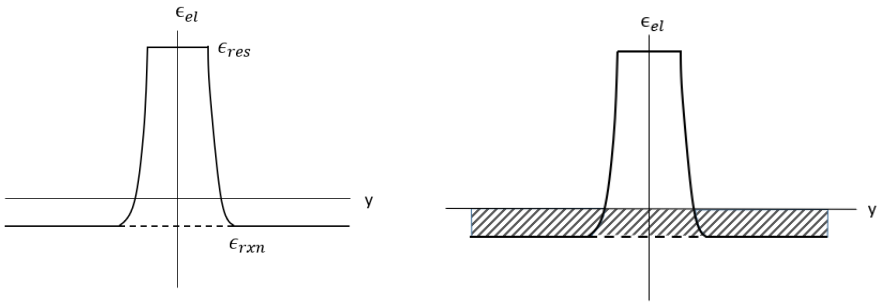

(a) Cross section residual strain and Reaction strain

(b) Area proportional to the tendon force

Figure 2.10: Residual elastic strain profile in a welded plate

The tendon force consists of a fictitious force longitudinally applied that would cause a strain equivalent to ε_{rxn} along the plate.

The horizontal axis of Fig. 2.10 represents the transverse length of the plate. The vertical axis is the elastic residual strain. Accordingly, the areas in the plane are proportional to the force associated with said strain. Positive ε causes tensile force, and negative ε causes compression force. By equilibrium condition, we have that 2A = B.

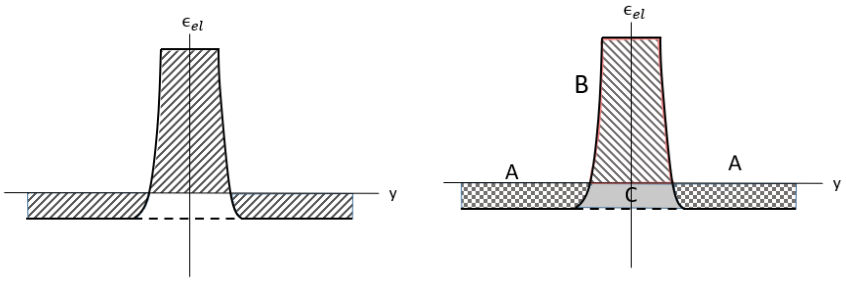

(a) Equilibrium condition between tensile and compresive zones

(b) Strain zones

Figure 2.11: Strain balance

The tendon force is proportional to the area 2 A + C defined by ε_{rxn}. Due to equilibrium condition that area is proportional to B + C that can be obtained as $\int_y \varepsilon_{res} - \varepsilon_{rxn} dy$. Tendon force is defined as:

$$F_{ten} \equiv \int_{A_c} E(e_{res} - e_{rxn}) dA \tag{2.12}$$

It is worth defining $e_{inh} = e_{res} - e_{rxn}$ which corresponds to the magnitude of plasticity. Since it occurs only in a finite area near the heat source trajectory, a powerful property of the inherent strain is that it can be calculated from heat source parameters, independent from the reaction of the base material.

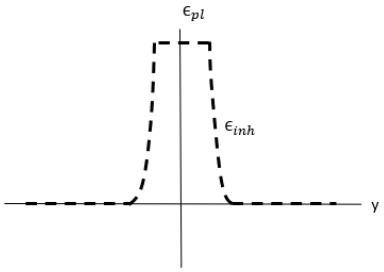

Figure 2.12: Inherent strain

Thus the tendon force can be written according to:

$$F_{ten} = \int_{A_c} E e_{inh} dA \tag{2.13}$$

And if the plate is of constant thickness d and modulus E:

$$\begin{aligned} F_{ten} &= Ed \int_y e_{inh} dy \\ &= Ed \int_{y_{pl}} e_{pl} dy \end{aligned} \tag{2.14}$$

Where:

$$y_{pl} = y_{max}(\Delta T_{Y1}) = \frac{1}{\sqrt{2\pi e}} \frac{\eta Q'}{d} \frac{1}{\rho c} \frac{1}{\Delta T_{Y1}} \tag{2.15}$$

The expression in 2.14 can be rigorously solved if the material properties are assumed to be constant during the thermal cycle. The development is in appendix A. and the result for the tendon force is:

$$F_{ten} = \sqrt{\frac{2}{e\pi}} \ln(2) \frac{E\alpha}{\rho c} Q' \tag{2.16}$$

A more exact expression for the force tendon is obtained by calculating the average values of the properties in the temperature range of the process:

$$F_{ten} = \sqrt{\frac{2}{e\pi}} \ln\left(\frac{\Delta T_{Y2}}{\Delta T_{Y1}}\right) \frac{E\alpha_{eff}}{(\rho c)_{eff}} Q' \tag{2.17}$$

In reference [6] are the expressions to calculate the effective values.

The equation above depends only of the welding heat input and material properties, its convenient to group all this material properties in a single parameter :

$$H = \sqrt{\frac{2}{e\pi}} \ln \frac{\Delta T_{Y1}}{\Delta T_{Y2}} \frac{E\alpha_{eff}}{\rho c} \tag{2.18}$$

Considering a material with both a CTE and yield strain that are independent of temperature the parameter H has a theoretical value of ≈ 0.22. [2]

Use eq. 2.17 requires greater knowledge of the properties of the material at different temperatures.

2.4. Calculation of stresses and distortion in pipeline weld root pass

Up to this point, the exposed results are for flat plates. Now corresponds to extrapolate these results in a cylindrical geometry that can have radial displacements. The analogy between these two geometries consists of thinking of the cylinder as a "wrapped" flat plate. Longitudinal stresses then became in hoop stress (stress in the angular direction).

Reference [7] assume that, initially, the residual stress pattern in the cylinder is given by the flat plate solution. So one might expect high hoop tensile stresses near the weld, lower hoop compressive stresses away from the weld and negligible axial stresses, then the welded cylinder is allowed to deform and the final configuration can be determined from the condition that its elastic strain energy will be a minimum.

After deformation, axial stress is also expected due to bending caused by the pipe deflection.

Figure 2.13 schematize the deflection that the pipe can suffer under residual hoop stress and the notation used in the following section.

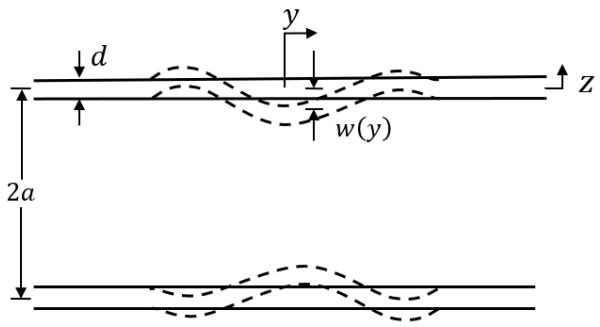

Figure 2.13: Schematic pipe deflection under uniform radial load

Table 2.3: Nomenclature for cylindrical and root weld calculations

Variable	M	Description
a	L	Pipe radius
ω	L	Radial deflection
d	L	Pipe thickness
z	L	Distance from the middle of the pipe wall
θ	-	Pipe angular coordinate
N_y	F/L	Distributed force in the axial direction
N_θ	F/L	Distributed force in angular direction
Q_y	F/L	Distributed shear force in axial face
M_y	FL/L	Linear momentum angular direction
Z	F/L	Radial load distributed over the shell
D	FL	Flexural rigidity of the shell
β	1/L	Notation from 2.31
ν	-	Poisson's Modulus
ϕ	-	Weld bead curvature
σ_y	F/L^2	Axial stress
σ_θ	F/L^2	Hoop stress
σ_H	F/L^2	Initial distribution of hoop stress
g	L	Root gap
c	L	Half root thickness
δ	L	Misalignment
r	L	Distance from the middle of the pipe wall
$\sigma_{b,max}$	F/L^2	Maximum stress at the weld bead
I_{root}	-	Susceptibility to failure due to weld root discontinuities index

2.4.1. Components of residual stresses

The solution of a circular cylindrical shell Loaded symmetrically with respect to its axis from [8] give some lights about how stresses behave.

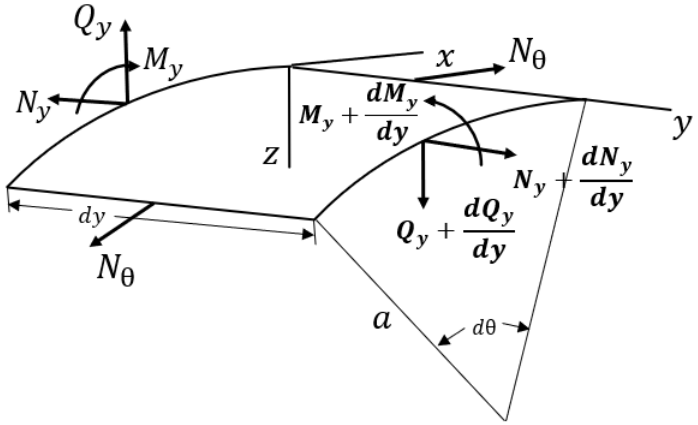

Figure 2.14: Cylindrical shell element under symmetrical load

The equilibrium equations for the element in Fig. 2.14 are:

$$\begin{aligned} \frac{dN_y}{dy} a dy d\theta &= 0 \\ \frac{dQ_y}{dy} a dy d\theta + N_\theta dy d\theta + Z a dy d\theta &= 0 \\ \frac{dM_y}{dy} a dy d\theta - Q_y a dy d\theta &= 0 \end{aligned} \tag{2.19}$$

Where Z is the radial load or the pressure distributed over the shell

The model in [8] consider that axial symmetry is preserved, there are no change of curvature in the circumferential direction and no external torsion nor axial load. Under such conditions the forces acting over the element are shown in fig 2.14. The equilibrium equations together with Hook's law leads to conclude that:

$$N_\theta(y) = -\frac{E d w(y)}{a} \tag{2.20}$$

Where ω is radial deflection d is the pipe thickness and a is the pipe radius. Giving a direct relation between the hoop stress and the radial distortion.

Even more, all the problems of symmetrical deformation of cylindrical shells reduce to the integration of the following equation:

$$\frac{d^2}{dy^2}\left(D\frac{\mathrm{d}^2 w}{\mathrm{d}y^2}\right)+\frac{Ed}{a^2}w=Z \tag{2.21}$$

Where D :

$$D=\frac{Ed^3}{12(1-\nu^2)} \tag{2.22}$$

is the flexural rigidity of the shell.

As it is a 2d solution neglects the effect on bending of axial stress σ_y this assumption it's understandable considering the overall $\int_A \sigma_y = 0$, nevertheless in pipeline welding, the maximum values of $\sigma_y(y,z)$ are a contribution to the susceptibility to fracture on the weld root.

Summarizing when the pipe is deflecting is not only releasing the initial residual hoop stress, but also generating axial stress by bending.

As figure 2.15 and equation 2.23 shows, the axial strain is related with the radial deflection w as follows:

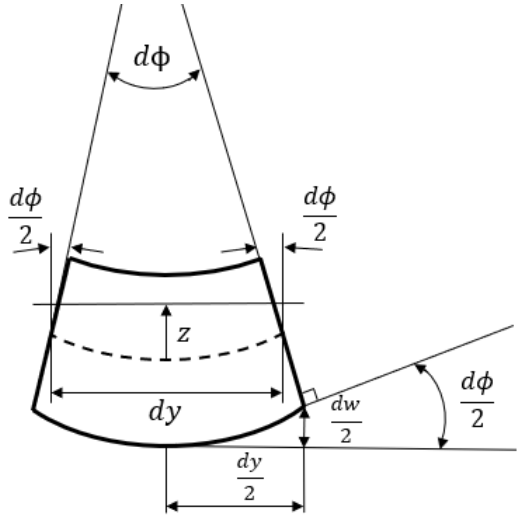

Figure 2.15: Axial strain from bending angle

$$\varepsilon_{yy}\approx\frac{-2z\frac{d\phi}{2}}{dy}\approx\frac{-2z\tan(\frac{d\phi}{2})}{dy}\approx\frac{-2z\frac{dw}{dy}}{dy}\approx-2w''z\Rightarrow\sigma_y\propto w''z \tag{2.23}$$

Reference [7] propose the following stress field due to circumferential welds:

$$\sigma_\theta(y,z) = \sigma_H(y) - \frac{Ew}{a} + \nu\sigma_y(y,z) \tag{2.24}$$

$$\sigma_y(y,z) = \frac{E}{1-\nu^2} w''z \tag{2.25}$$

Where σ_θ is the total hoop stress and σ_y its the axial stress in y direction.

The strain energy is:

$$U = 2\pi a \int_{-\infty}^{+\infty} \int_{-d/2}^{+d/2} \frac{1}{2E}(\sigma_y^2 + \sigma_\theta^2 - 2\nu\sigma_y\sigma_\theta) dz dy \tag{2.26}$$

In other words:

$$U = \int_{-\infty}^{+\infty} F(y, w, w'') dy \tag{2.27}$$

We are looking for the deflection $w(y)$ that complies with 2.21 and minimizes U. Its no coincidence thus that the solution to min U from 2.27 is the Euler differential equation [9]:

$$\frac{d^2}{dy^2}\left(\frac{\delta F}{\delta w''}\right) + \frac{\delta F}{\delta w} = 0 \tag{2.28}$$

Getting:

$$\frac{d^2}{dy^2}\left(Dw''\right) + \frac{Ed}{a^2} w = \frac{d}{a}\sigma_H(y) \tag{2.29}$$

$$w^{(4)} + 4\beta^4 w = \frac{d}{aD}\sigma_H(y) = \frac{P}{D} \tag{2.30}$$

Where:

$$\beta^4 = \frac{3(1-\nu^2)}{a^2 d^2} \tag{2.31}$$

The development between 2.28 and 2.29 is include in the appendix 2.

Thus the problem of solving for the radial deflection $w(y)$ which minimizes the strain energy of the welded pipe reduces to the straightforward problem of calculating the deflection $w(y)$ due to an

equivalent radial loading of $\frac{d}{a}\sigma_H$. [7]

2.4.2. Solution of distortions for a cylinder radially loaded at the end

The most determinant aspect of pipeline residual stresses is the solid-state thermal distortion at each side of the weld. The weld bead doesn't cause much resistance to the distorted end of the pipe. According [2] the effect of the residual stress in the pipe geometry can be estimated as a shearing force of magnitude $P = \frac{\mathscr{F}_{ten}}{2a}$ on each side of the weld.

Thus solving eq. 2.21 with the boundary conditions of fig. 2.16 will be the first approach to predict distortions in pipeline welding.

Its known from [8] that the solution of the differential eq.2.21 is:

$$\omega = e^{-\beta y}(C_1 \cos\beta y + C_2 \sin\beta y) + e^{\beta y}(C_3 \cos\beta y + C_4 \sin\beta y) + f(y)$$

Since the residual stress produce a local bending which dies out rapidly as the distance y from the heat source increases, we conclude that $C_3 = C_4 = 0$.

$$\omega = e^{-\beta y}(C_1 \cos\beta y + C_2 \sin\beta y) \tag{2.32}$$

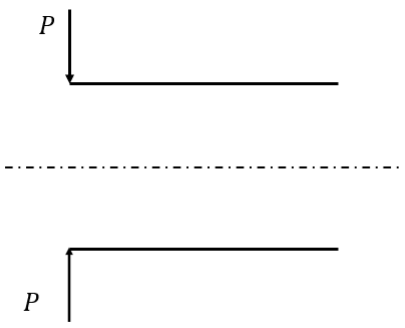

Figure 2.16: Boundary conditions for a cylinder with radial load P

The solution of eq. 2.32 under this boundary conditions is: [8]

$$\omega = -\frac{1}{2\beta^3 D} P e^{-\beta y} cos(\beta y) \tag{2.33}$$

$$\frac{d\omega}{dy} = \frac{1}{2\beta^2 D} P e^{-\beta y}(cos(\beta y) + sin(\beta y)) \tag{2.34}$$

$$\frac{d^2\omega}{dy^2} = -\frac{1}{\beta D} P e^{-\beta y} sin(\beta y) \tag{2.35}$$

Consideration of the tendon force as a concentrated line load is only suitable if the plastic strain zone from welding is relatively small compared to the characteristic length $1/\beta$[2]. Having the solution of the problem for the case in which a load is concentrated at a circular section, we can readily solve the more exact problem of a certain load $p(\xi) = \frac{d}{a}\sigma_H(\xi)$ distributed along the cylinder by applying the principle of superposition.

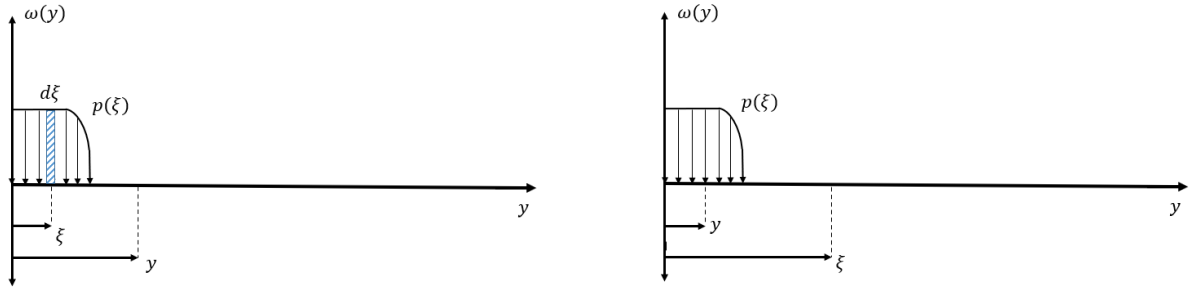

(a) Equivalent load at integration parameter parameter $\xi < y$

(b) Equivalent load at integration parameter parameter $\xi < y$

Figure 2.17: Equivalent loading conditions caused by residual stresses

$$\omega(y) = -\frac{1}{2\beta^3 D}\int_0^y p(\xi) e^{-\beta(y-\xi)} cos(y-\xi) d\xi + -\frac{1}{2\beta^3 D}\int_y^\infty p(\xi) d\xi e^{-\beta(\xi-y)} cos(\xi-y) d\xi \tag{2.36}$$

Equation 2.36 first requires a explicit result for $p(\xi)$ .Taking advantage of the analysis of the tendon force, the load $p(\xi)$ is well approximate as a constant distribution of the tendon force over a critical length y_c [2].

$$p(y) = \begin{cases} \dfrac{F_{ten}}{2ay_c}, & y < y_c \\ 0, & y > y_c \end{cases} \tag{2.37}$$

Considering the plastic strain distribution used to integrate the tendon force, the appropriate critical length is:

$$y_c = ln(2) y_{pl} \tag{2.38}$$

2.5. Susceptibility index to assess the influence of joint fit-up on pipeline weld root discontinuities

Grams in ref. [2] introduce a way to calculate the failure susceptibility of the pipe weld by calculating the total angular distortion of the weld bead.The propensity for latent discontinuity formation is proportional to the magnitude of the strain at the weld root which is related to its amount of bending and in turn is proportional to the angular distortion of the pipe. Specifically the resulting angular distortion of the weld bead it's 2 times the angular distortion evaluated at the end of the pipe as illustrated by fig. 2.18.a

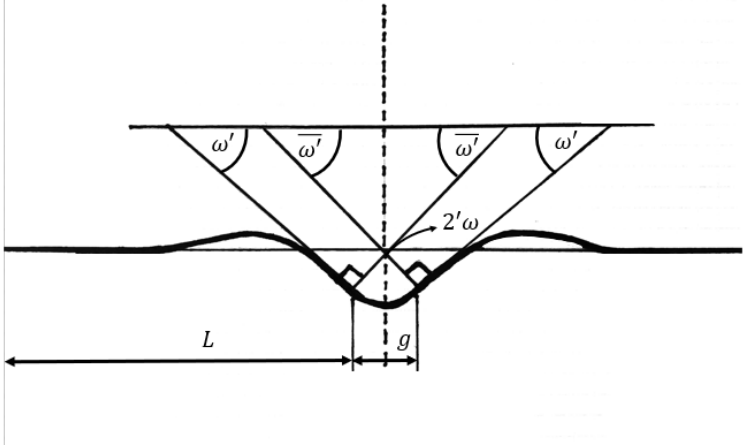

(a) weld bead curvature angle

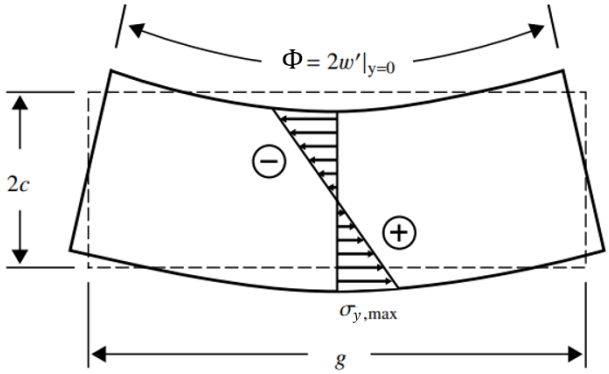

(b) Stress distribution resulting from 1d beam approximation of weld root pass

Figure 2.18: Resulting weld bead geometry and stress

In a first stage, this approach consist on calculate the shrinkage experimented for one side due to a given heat input applying the tendon force as a concentrated circumferential load P at the end of the cylinder.

The resulting maximum root strain [4] depends on the weld bead dimensions and its angular distortion.

In ref. [2], the relationship between the root strain and deflection is fit to the following power law:

$$\frac{\sigma_{b,max}}{E} = \frac{\phi}{2} \cdot m \cdot \left(\frac{c}{g}\right)^n \tag{2.39}$$

Where $m = 0.625$ and $n = 0.5$ according to [2].

In a second stage it requires the calculation of the following correction factors:

- f_D That consider a more accurate distribution of the residual stresses.
- f_M that takes into account the resistance caused by the weld bead bending against the pipes distortion, that introduce a bending moment into the boundary conditions to the pipe.
- The stress concentration factor f_G caused by the offset present in the Joint fit-up.

The index has the following expression:

$$I_{root} \approx \frac{\sigma_{b,max}}{E}$$

$$I_{root} = \frac{H\eta Q' c^{0.5}}{E d^2 g^{0.5}} \cdot \frac{f_D \cdot f_M}{f_G} \tag{2.40}$$

Both f_D and f_M are explained in detail on ref [2]. This work won't focus on any of them. However the equation 2.41:

$$f_M(\Pi_2) = \frac{1}{1+\Pi_2} \tag{2.41}$$

$$\Pi_2 = \frac{8(1-\nu^2)}{\beta d}\left(\frac{c}{d}\right)^2 \cdot m \cdot \left(\frac{c}{g}\right)^n$$

[4] strain at the base of the weld i.e. inside the pipe where the cracks usually begins

2.5.1. Stress concentration factor due misalignment

The fabrication tolerances can generate additional stress. A simple 2d example is given in fig. 2.19. The tolerances in two plates results in a misalignment of the neutral axis. Under axial load, the off set at weld cause a bending moment $M = F\delta/2$ resulting in additional axial stress $\sigma_b = M/S$ where $S = d^2/6$ is the section modulus.

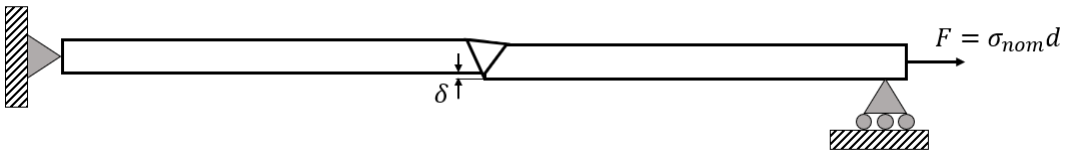

Figure 2.19: Stress concentration factor example

$$\sigma_b = \frac{F\delta}{2} \Big/ \frac{d^2}{6} = \frac{3\delta}{d}\sigma_{nom}$$

One can define a stress concentration factor to get the maximum stress from the nominal stress such that $0 \leq f_G \leq 1$ in this situation would be:

$$\sigma_{max} = \sigma_{nom} + \sigma_b = \sigma_{nom}\left(1 + \frac{3\delta}{d}\right) = \frac{\sigma_{nom}}{f_G}$$

$$f_G = \frac{1}{1 + \frac{3\delta}{d}}$$

In pipe line welding fabrication tolerances as local pipe radius mismatch Δa or ovality combined with local wall thickness mismatch Δd cause the total offset $\delta = \Delta a + \Delta d$ illustrated in fig. 2.21.b

The weld bed experiment bending moment caused by the pipe deflection. Similarly at what occurs in the example of fig. 2.19 the maximum stresses reached due to the external bending moment will be affected by the amount of curvature introduced by the offset.

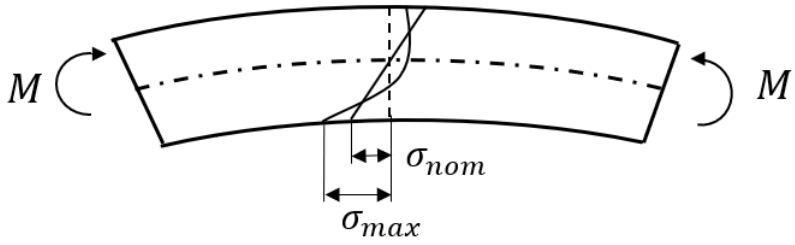

Figure 2.20: stress profile in a blended element

The correction factor that will be evaluate in this work comes from ref. [2] is obtained by fitting a power law of the form $1+ax^{-}b$ and depends on the normalized ratio of curvature c/r .

$$f_G = \frac{1}{1+1.29(\frac{c}{r})^{1.362}} \tag{2.42}$$

$$r = c + \delta\frac{\sqrt{1+(g/\delta)^2}}{2\sin(\phi/2)}, \phi = \pi - 2\tan^{-1}(g/\delta)$$

Where:

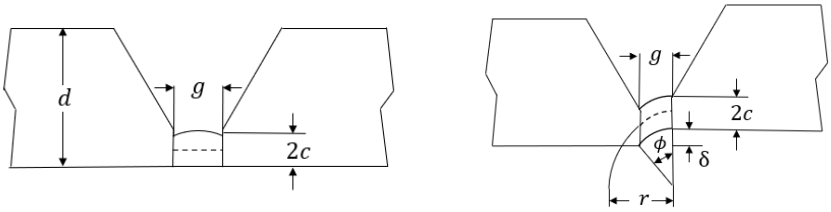

(a) Dimensions of the weld bead

(b) Geometric description of the misaligned weld

Figure 2.21: Misaligned weld root pass geometry

Chapter 3

Methodology

The first stage of this work is to reach a level of understanding on the available equations that predict welding phenomena such as the temperature, the distortions and the residual stress. To perform this in the allotted time is necessary to identify what is sufficiently related to pipeline arc welding processes. During this process several numerical models of cylindrical welds where perform in Simufact welding to understand the operation of the software and the benefits of its use as a means of validation.

The next stage is to expose and explain the fundamental elements that serve to explain the models that are capable of predicting the residual efforts. During this process intermediate calculations of appendix were remade A and B, in order to make this text accessible and detect possibles contributions to the model. In this way arise the modifications analytical solution for radial displacements and stress after a cylindrical weld.

The numerical results are perform trough a study case, that represent a simplified representation of a real pipe line welding process, where the analytical model previously presented is valid.

The following is a description of the procedure to be used in the case study:

- Set a geometry based in welding procedures of cross-country gas and oil pipeline, using dimensions that can be well approximated by the assumptions of available equations.
- Set the heat input based on the welding parameters from the chosen procedure.
- Take advantage of the symmetry and the knowledge of the zones that do not suffer deformations to create a simplified numerical model.
- Choose a material used in pipe construction and available in the Simufact library.
- Characterize the material using the data available in the description of the selected material from the library.
- Generate a mesh properly refined near from the heat input trajectory.

- Calculate solutions for displacements using analytical results and measure the solutions provided by the numerical model and get error measurements.
- Calculate solutions for σ_y and σ_θ that describe the state of the pipe after being welded.
- Present the numerical results for the stress, in such a way that they can be compared with the analytical solutions.
- Calculate the effects of pipe distortions and misalignment on weld root residual stress.

Chapter 4

Results

4.1. Analytical proposed solution for radial displacements

This section is focus on describing the radial displacements ω and the stress components σ_θ, σ_y of a cylindrical shell after a single weld pass.

Inspired in reference [8] and [7], this section introduce a different solution to estimate ω.

From reference [8] and eq. 2.23 we have:

$$\varepsilon_\theta = -\frac{w}{a} \qquad\qquad \varepsilon_y = -2\omega'' z$$

For symmetry and the boundary conditions in pipe line welding its assumed that there is no torsion so there are only displacements in the y and z direction of fig. 2.14. Then Hook's law can be written as:

$$\sigma_y = \frac{E}{1-\nu^2}(\varepsilon_y + \nu\varepsilon_\theta) \qquad\qquad \sigma_\theta = \frac{E}{1-\nu^2}(\varepsilon_\theta + \nu\varepsilon_y) \tag{4.1}$$

Replacing the results for the strains ε_θ and ε_y and adding σ_H to the angular component on 4.1 we obtain:

$$\sigma_y = \frac{E}{1-\nu^2}(\varepsilon_y + \nu\varepsilon_\theta) = \frac{E}{1-\nu^2}\left(2zw'' - \nu\frac{w}{a}\right) \tag{4.2}$$

$$\sigma_\theta = \frac{E}{1-\nu^2}(\varepsilon_\theta + \nu\varepsilon_y) + \sigma_H = \frac{E}{1-\nu^2}\left(-\frac{w}{a} + 2\nu z w''\right) + \sigma_H \tag{4.3}$$

From here, by minimizing the strain energy, we arrive at the following result(see appendix 3 and 4):

$$\frac{d^2}{dy^2}\left(4Dw''\right) + \frac{Ed}{a^2}w = \frac{d}{a\alpha}\sigma_H(y) \tag{4.4}$$

Where $\alpha = \frac{(1-\nu)}{(1-\nu^2)} \approx 0.77$

$$w^{(4)} + \frac{Ed}{4Da^2}w = \frac{d}{4Da\alpha}\sigma_H(y) \tag{4.5}$$

Defining:

$$\beta'^4 = \frac{\beta^4}{4} \Leftrightarrow \beta' = \frac{\beta}{\sqrt{2}} \tag{4.6}$$

$$D' = 4\alpha D \approx 3D \tag{4.7}$$

$$p(y) = \frac{d}{a}\sigma_H(y) \tag{4.8}$$

$$w^{(4)} + 4\beta'^4 w = \frac{p(y)}{D'} \tag{4.9}$$

$$\omega = -\frac{1}{2\beta'^3 D'} Pe^{-\beta' y} cos(\beta' y) \tag{4.10}$$

$$\frac{d^2\omega}{dy^2} = -\frac{1}{\beta' D'} Pe^{-\beta' y} sin(\beta' y) \tag{4.11}$$

4.2. Case study

By using this notation, the solutions can be tested both ways with β and D and β' and D'. This will be conducted by the concrete example described bellow.

Table 4.1: Dimensions case study

Pipe	Parameter	Magnitud [mm]
Length	L	1000
Radius	a	450
Wall Thickness	d	6

Table 4.2: Case study welding parameters

Travel speed	5.5 $[mm/s]$
Amperage,I	165 $[W]$
Voltage, V	30 $[V]$
Heat input, Q'	0.4$[KJ/mm]$
Efficiency, ν	0.9

This particular magnitudes are chosen to emulate a concrete pipeline welding procedure, considering half of the total heat input goes to each side of the pipe.

The properties listed bellow are taken from a material identified as $S235-SPM_{sw}$ on the Simufact material library created in JmatPro by J. Sakkiettibutra.

Table 4.3: Study case Material properties at 25°C

AINSI	1311
Young's Modulus E	210.627$[Gpa]$
Poisson ratio,ν	0.3
Coef. Thermal expansion,CTE	1.258e-05 $[1/K]$
Density,ρ	7852.17$[Kg/m^3]$
Yield stress, σ_y	235 $[Mpa]$
Specific Heat, c	0.446 $[J/(g \cdot K)]$
Thermal conductivity,	54.94$[W/(mK)]$
Initial phase fraction	93% ferrite 7% perlite

The theoretical calculated values shown in table 4.4 are obtain using the theoretical value of $H = 0.22$ [6] for steels and equations: 2.21, 2.30, 4.6 and 4.7

Table 4.4: calculated values

D	5.41613e06$[N \cdot mm]$
D'	1.6682e07$[N \cdot mm]$
β	2.4738e-02$[1/mm]$
β'	1.7492e-02$[1/mm]$
F_{ten}	79200$[N]$
P	88$[N/mm]$

4.2.1. Numerical simulation results

Thermo-mechanical solution of the following mesh

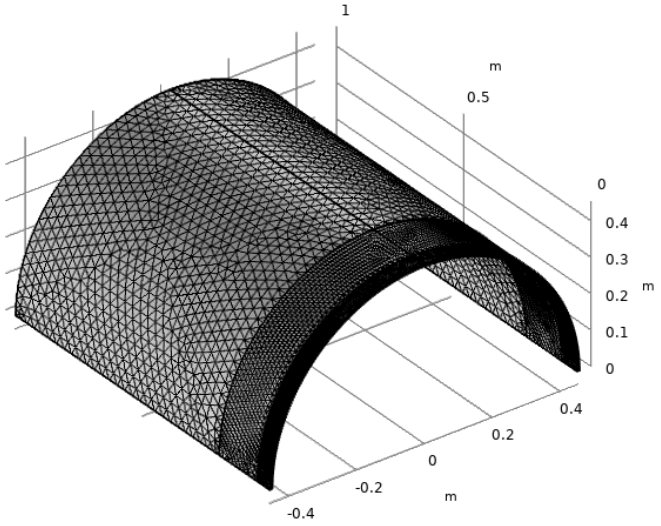

(a) Home view

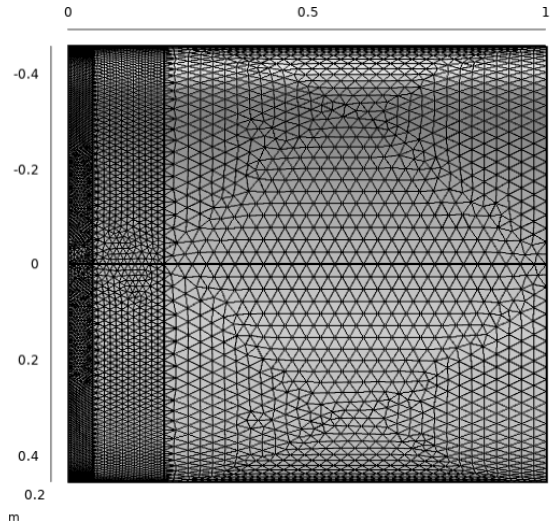

(b) Upper view

Figure 4.1: Geometry and meshing used in study case 1

In this numerical simulation material properties are function of the temperature, the exact values used are in appendix F

The welding trajectory is shown in fig. 4.2

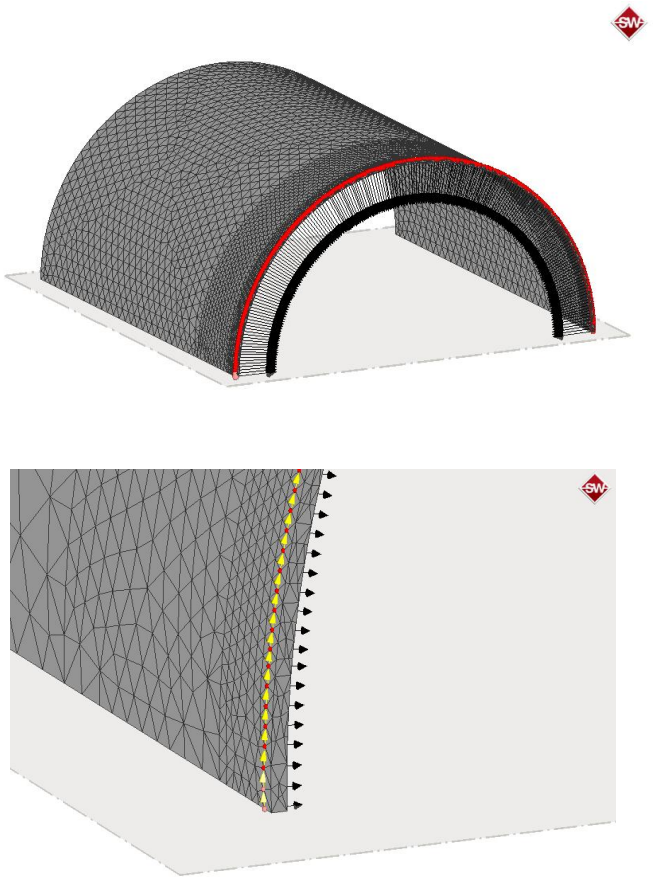

Figure 4.2: Heat source trajectory

The resulting welding time is 4.24 min. and the distortions measurements are taken after 15min cooling as shown in fig.4.3

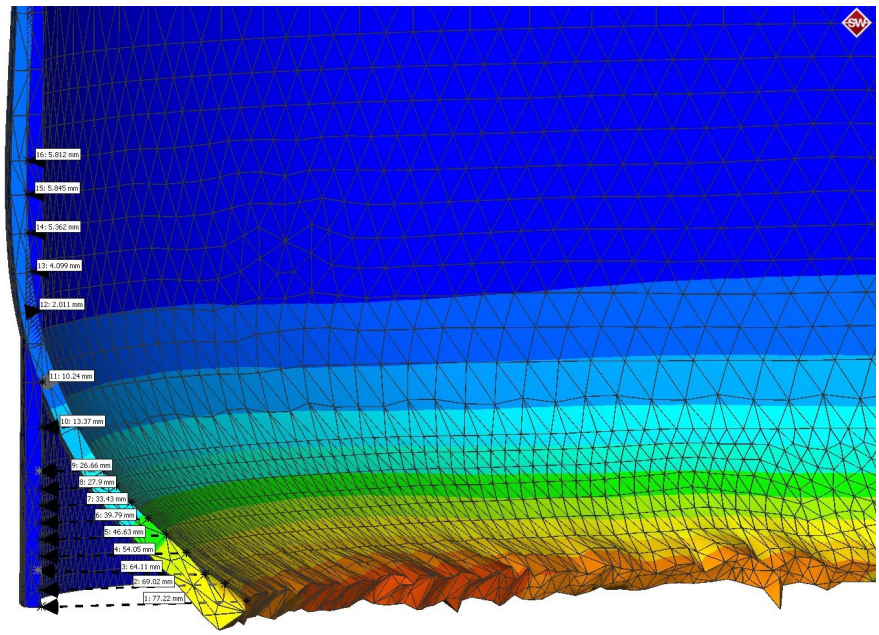

Figure 4.3: Nodal displacement (x150) measurements

The nodal displacements are measured the first 30$[cm]$ at both sides of the half pipe, after that in this example the displacement are negligible. Two data set from the final state of the simulation are available on the appendix E and are used in figs 4.4 and 4.5 .

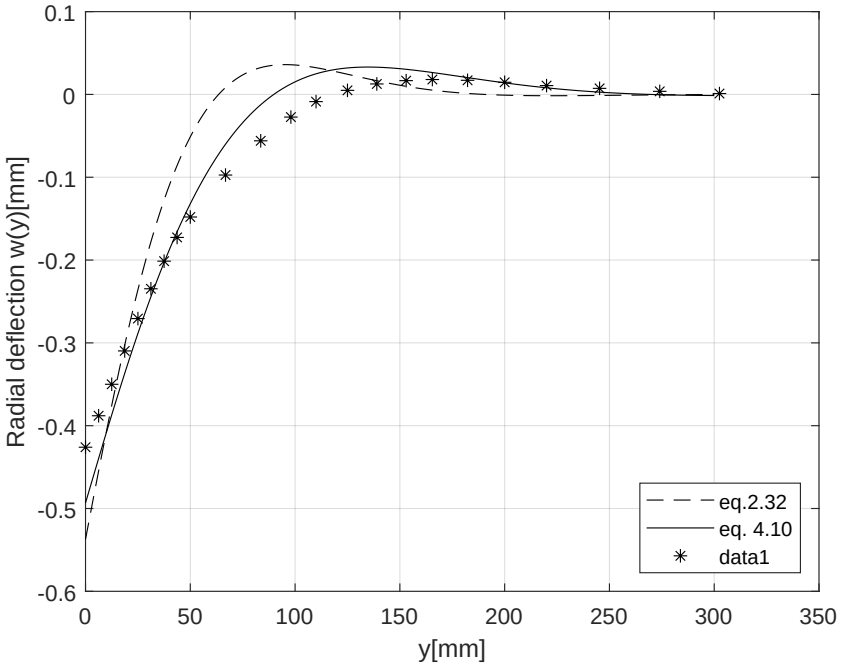

Figure 4.4: Predictions and numerical results for the radial displacements at the beginning point of the weld trajectory

Obtaining a mean quadratic error of $0.0417[mm]$ for the original equation 2.33 and $0.0306[mm]$ for the modified eq. 4.10 on the first 300[mm]

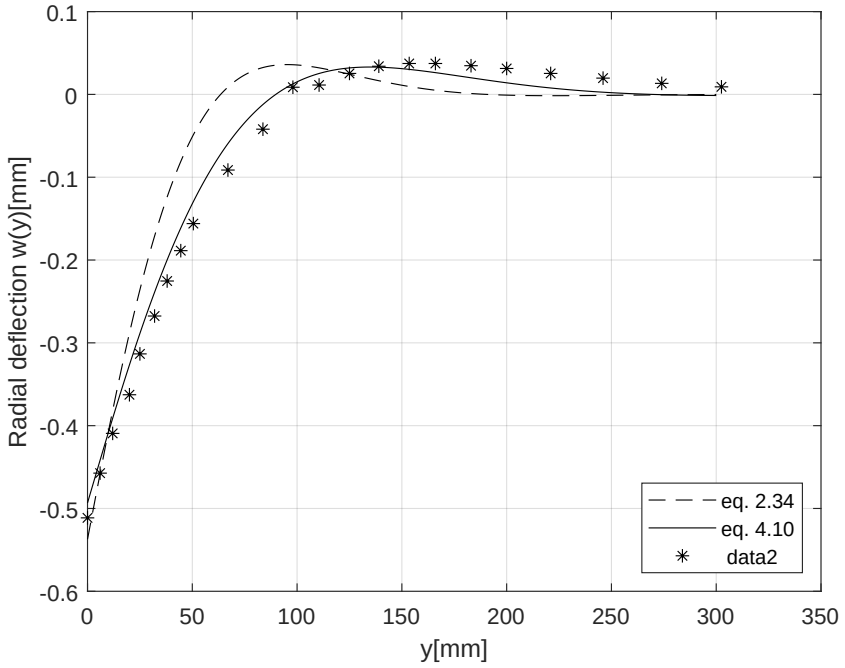

Figure 4.5: Predictions and numerical results for the radial displacements at the ending point of the weld trajectory

Obtaining a mean quadratic error of $0.0459[mm]$ for the original equation 2.33 and $0.0108[mm]$ for the modified eq. 4.10

Despite the previous results prove that for this particular example the approximation of the concentrated load its accurate enough, in order to obtain σ_θ it is necessary to calculate σ_H, using $p(y)$ from 2.37 we obtain:

$$\sigma_H = \begin{cases} \dfrac{\sqrt{2\pi e}}{2\ln 2}\dfrac{F_{ten}}{\nu Q'}\rho c\Delta T_{Y_1}, & y < y_c \\ 0, & y > y_c \end{cases} \tag{4.12}$$

The first yielding temperature can be calculated by iterating the following equation:

$$\Delta T_{Y_1} = \frac{\sigma_y}{E\alpha} \tag{4.13}$$

The average value for pipeline welding steel $\Delta T_{Y_1} = 210[K]$ from [2] is use for the calculation of σ_H.

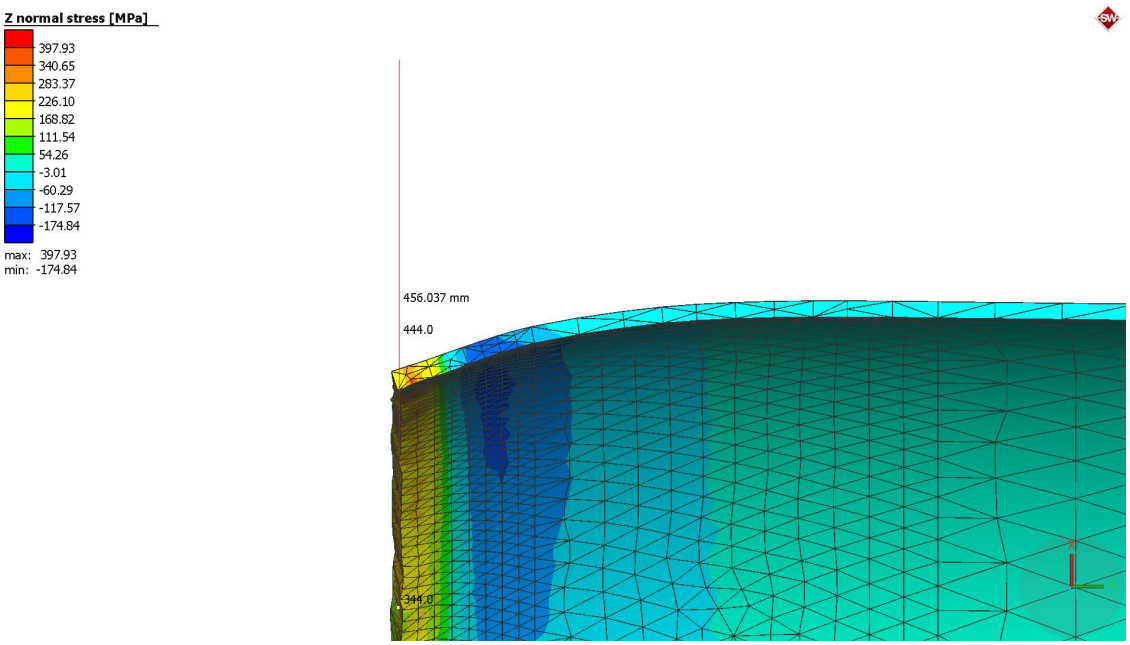

Figure 4.6: Numerical results for normal stress in Z direction σ_{zz}. Seen at (a,y,0) $y \in [0, 300]mm$.

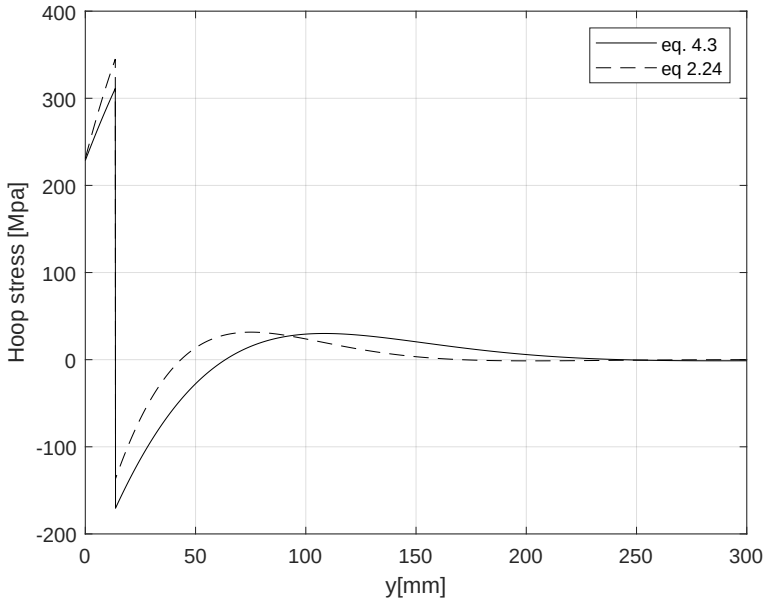

Figure 4.7: Predicted hoop stress σ_θ

Table 4.5: Extreme values for hoop stress following the analytical equations of ref. [7], eq. 4.3 and the numerical simulation results

	Eq.results	Eq.ref	FEM
σ_θ max[Mpa]	311.29	345.06	397.93
σ_θ min[Mpa]	-170.49	-136.6	-174.84

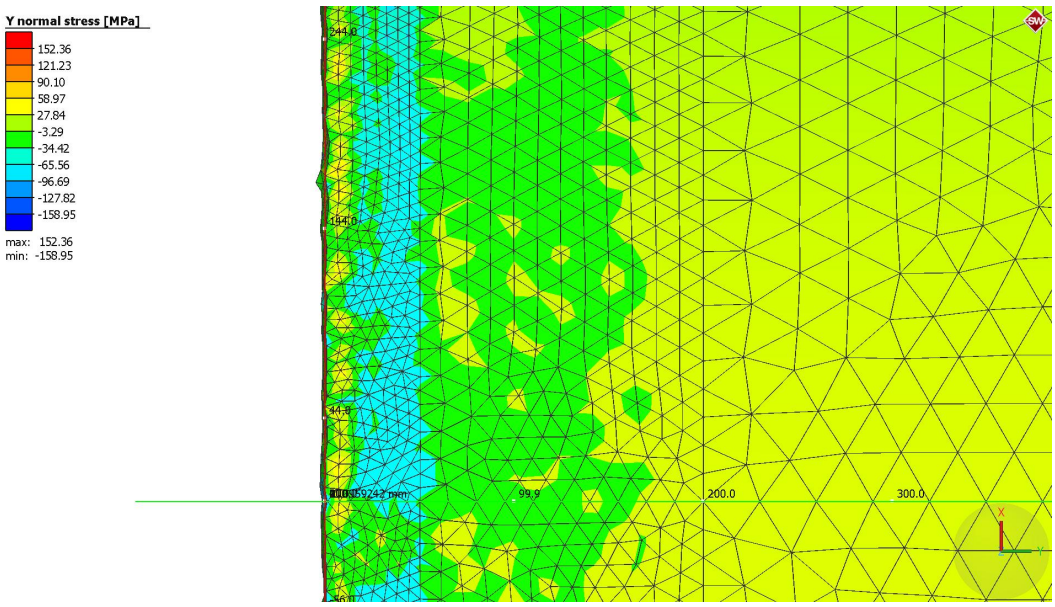

Figure 4.8: Numerical results for normal stress in y direction equivalent to the axial stress

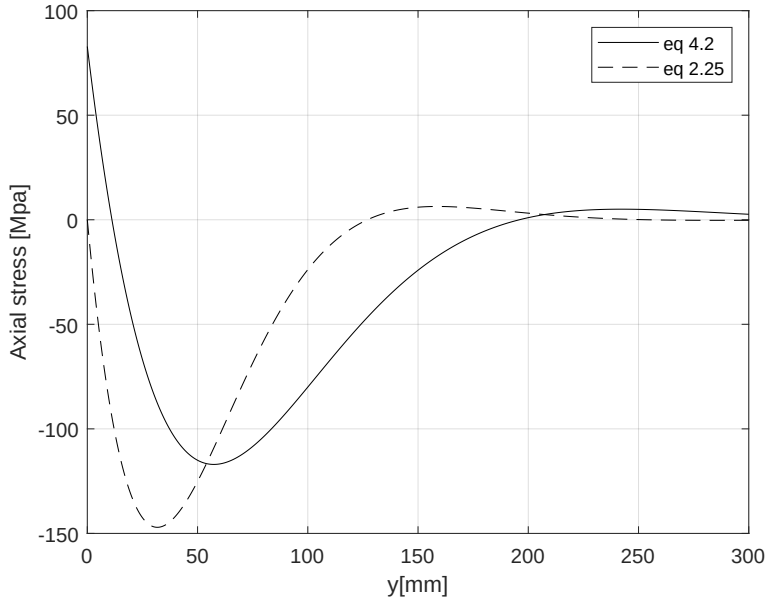

Figure 4.9: Predicted axial stress in inner face of the pipe

Table 4.6: Extreme values for axial stress following the analytical equations of ref. [7] and the equation 4.2

	Eq.result	Eq.ref	FEM
σ_y max[Mpa]	76.11	6.35	152.36
σ_y min [Mpa]	-114.7	-147.08	-158.95

4.3. Effects of pipe distortions and misalignment on weld root residual stress

The curvature of the weld bed is:

$$\phi = 2\omega_0' = 2\frac{1}{2\beta^2 D}P \tag{4.14}$$

Using equation 4.16 the maximum strain at the weld root pass is :

$$I_{root} = \frac{\phi}{2} \cdot m \cdot \left(\frac{c}{g}\right)^n \frac{f_M \cdot f_D}{f_G} \tag{4.15}$$

On this example, the solution for the displacements are so precise by using the concentrated load P that it is consider accurate to consider $f_D \approx 1$.

$$I_{root} = \frac{1}{2\beta^2 D}P \cdot \frac{5}{8} \cdot \left(\frac{c}{g}\right)^{1/2} \frac{f_M}{f_G} \tag{4.16}$$

By using the results of table 4.4 and eq. 2.41,2.42 and 4.16 we will calculate the I_{root} for two different weld root pass dimensions.

Table 4.7: Dimensions of the weld root pass

Dimension	Procedure A	Procedure B
g	2	3
c	1	1
δ	0.6	0.05
r	4.633	91.02

Table 4.8: Results for maximum strain

Results	Procedure A	Procedure B
f_M	0.684	0.726
f_G	0.863	0.997
I_{root} [mm/m]	9.3	7
I'_{root}[mm/m]	6	4.5

Chapter 5

Discussions

5.1. Analytical solution for radial displacement in circumferential welds

The presented solution for this problem uses the methodology of [7] however it begins from a different stress field. The first thing to discuss is the approach of equations 4.2 and 4.3. This stress field proposal considers the 2d Hooke's law from eq. 4.1 and add the longitudinal residual stress in the θ direction. Equation 4.1 considers ε_r equal zero, in other words, it assumes constant radial displacement through the thickness $\frac{\partial \omega}{\partial r} = 0$. Therefore the solution is valid if the ratio of pipe radius/wall thickness is sufficient to be treated as a thin shell. The next important step is the relationship between displacement and strain. The axial strain expression, $\varepsilon_y \approx 2\omega''z$ uses the 2d bending analysis of figure 2.15. The angular strain is consider as $\varepsilon_\theta \approx \frac{1}{r}\frac{\partial u_\theta}{\partial \theta} + \frac{\omega}{a} \approx \frac{\omega}{a}$ considering that there is no torsion nor displacements on the θ direction, this is a strong symmetry assumption that is accurate far from the beginning of the weld where the heat transfer is stationary. This is confirmed by observing the quality of the solution far from the start 4.5 that has an error smaller than the solution right at the beginning of the weld start 4.4 where the model drops its performance.

Even if the stress field proposed is seemingly different from the one used in the reference, after the strain energy minimization[5], the solution arrives at the same function for the displacements but with different parameters D and β. The obtained flexural rigidity of the shell is $D' \approx 3D$, and the geometric parameter is $\beta' = \frac{\beta}{\sqrt{2}}$, smoothing out the effects of sine on the deflection shape. The obtained maximum deflection $\omega' \approx \frac{2\sqrt{2}}{3}\omega_0 \approx 0.918\omega_0$. The use of modified parameters β' and D' improves the behavior of the equation independently of the precision in the calculations used in the equivalent load P caused by the longitudinal residual stresses caused by the welding process.

[5] see appendix C

As shown in figure 4.5 and 4.4, the results are consistent with the thermo-mechanical solution for equivalent parameters on Simufact, which uses the FEM with a detailed description of the properties of the material at different temperatures available on appendix F. The performance of the results is remarkable, shows that, at least for the displacement calculations of the case study, the following approximations are well-posed:

- The effect of the residual stress in the pipe geometry is estimate as a shearing force of magnitude $P = \frac{F_{ten}}{2a}$ on each side of the weld.
- Considering a material with both a CTE and yield strain independents of temperature, namely, use the theoretical value of the parameter $H \approx 0.22$. Therefore was unnecessary for the use of eq. 2.17.

5.2. Numerical simulation

Concerning the reliability of the numerical models, although the work presents results for a single mesh and a sensitivity analysis was not carried out, multiple meshes were carried out for the same procedure, obtaining, at first glance, equivalent results. The one shown is the one that provides the smoother solution. Simulations with similar meshes gave the same deflection profile but more nodes with deviations from the average behavior, as shown in fig 5.1.

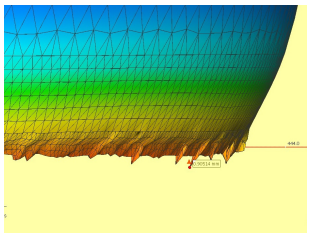

Figure 5.1: Results for case study 1A using dynamic meshing refinement

Between the different simulated processes and geometries, the case study is the only one whose simplifications were sufficient to obtain stable and consistent results to compare rigorously with the equations. Whereby simulations of the distortions in the fusion zone of the weld root pass are not included.

Using these approximations the obtained results have mean quadratic errors of the order of $10^{-2}[mm]$ (Between the data of appendix E and the equations that predicts the radial displacements w). It means that for general steels in pipeline welding processes where the pipe can be considered as a semi-infinite shell, it is possible to obtain fast estimations of the distortions by using the welding input information, radius and thickness of the pipe and the general properties of the material.

5.3. Solutions for the stress in the pipe

The rigorous analysis of this section is hampered by the impossibility of extracting the nodal values for the stress on the software.

Is expected that as it happens visibly in some nodes for the displacement solution the maximum stress values are exaggerated by anomalies in the numerical solution. However, these anomalies don't affect the general behavior of the results. Ranges for the stress results can be inferred from the figures 4.6 and 4.8. For clarification, the hoop stress σ_θ is equal to the normal stress in Z direction when looking at the positions $(a, y, 0) \forall y$ as in figure 4.6.

The heat map of the axial stress σ_y shows important differences with its extreme values, shows a small zone of maximum stress at the beginning of the pipe in the range [58.97, 90.10] and a big zone of negative stresses between [-34.42, -96.69]. In the case of hoop stress σ_θ the heat map of figure 4.6 indicate small zones of maximum σ_θ in a range [340.65, 397.93] $[Mpa]$ and big zones of minimum stress between [-117.57 -174.94]$[Mpa]$. In this case, the numerical results of extreme values don't correspond precisely with eq. 4.3-4.2, however, they adequately describe the heat maps qualitative behavior.

The main shortcoming of the equations used here is the definition of σ_H as a step function which generates the jump in the solution for σ_θ as shown in fig 4.7, a softer definition for the residual stress σ_H could arrive to a better description. A possible candidate is to use a distribution similar to the plastic strain of eq. 2.11, but this would require the calculation of the thermal distribution first, so this process would not have the advantages of using tendon force analysis.

5.4. Maximum strain on the weld root pass

In this discussion is necessary to clarify that the index I_{root} is a calculation for the strain at the weld bead. It is related with the stress, but not directly, because the predicted strain is bigger than the yielding strain. For example, the obtained I_{root} in procedure A is $9.3[mm/m]$, which is equivalent to a strain of 0.93%. To contextualize the electrode E6010 commonly used in root passes has to be able to stand at least 22% of elongation according to the AWS, its yield strength is $432[Mpa]$ and its ultimate tensile strength is $504[Mpa]$ as welded.

Regarding the differences in the I_{root} results when using D' and β', they occur because the analytical proposed solution generates smaller angular distortion at the weld position ω_0' this translates specifically into a systematic modification on the calculation of I_{root} by a factor of $\approx \frac{2}{3}$.

All the obtained I_{root} results indicate a maximum stress at the weld bead between yielding and

the ultimate stress (432-504 $[Mpa]$). Estimate precise value for the maximum stress caused by the calculated amount of strain would be necessary to use the flow curves of the welding filler material. It is worth mentioning that in the following passes of pipe welding, more resistant electrodes (e.g. E8010) are commonly used, and its higher temperatures help to alleviate the residual stresses and to reinforce the union.

This results justify why it is on the inner face of the weld root pass where failures usually start.

5.4.1. Comments on the use of correction factors

The I_{root} index as shown on equation 4.16 uses two correction factors that were not explained in depth. The correction factor f_D takes into account the distribution of the virtual load caused by the residual stress wasn't necessary for this work since the prediction of radial displacements obtained by using the concentrated load P was sufficiently precise. For more critical geometries its use can be replaced by the use of the more precise and tedious equation 2.36.

Regarding the correction factor f_M, its use change dramatically the final value of I_{root}, since it considers the effect of the moment in the weld root that changes the boundary conditions of the deflection problem in the pipe. Its use is acceptable for joints whose ratio $c/D << 1$ (such as pipeline welding), but for other processes in cylindrical welds it would be convenient to solve for 2.32 for different boundary conditions.

Chapter 6

Conclusions

According to the presented work and its results, the main objective was accomplished. As shown in the previous sections a numerical model of the distortions and residual stresses on pipeline welding was built. The model was consistent with the theoretical predictions. Some aspects of the theory as the tendon force analysis were successfully validated for the study case as it effectively allow to translate thermal variables to their mechanical effects. Other aspects were even modified, as the predictions models for the deflection profile due to cylindrical displacements.

The proposed equations are well related to the numerical simulation results, and together with the concepts used, they contribute to the understanding of the phenomenon of residual stress at the base material in pipe welding, by a simplified model that it's collecting only the most important effect of weldment distortions into the solid mechanics of the thin pipe.

However, it would be convenient to continue with the numerical models to obtain more preliminary information about what happens in detail in the weld root pass focusing the research efforts at temperatures where the constitutive equations doesn't apply, a 2D approach is suggested for this purpose, taking advantage of the assumption of axial symmetry. In the meantime the use of equation 2.39 is waiting to be numerically tested.

The equations that predict displacement are ready to be tested experimentally. The radial distortions of the pipe profile can be directly and rigorously measured. The most interesting part is that the displacement equations use a certain stress field therefore if the displacement corresponds with exactitude to the predictions It is possible to conclude that the predictions for the stress are correct.

This work could serve as a basis to build a methodology that can be used to make a preliminary failure susceptibility study for each procedure that is intended to be designed for pipe line welds of special sensitivity in industries that require high reliability and durability.

All cylindrical welds are to some extent related to the concepts here presented, and in future

work would be interesting to test and modify these equations using simulations with a non-thin geometry ($a/d < 20$) and a wider range of thermal solutions available in the literature. When equations manage to predict the displacement profile due welding in thick geometries, a variety of processes can be considered, by changing heat inputs, boundary conditions and materials properties. In this ambit, a first extension would be considering a model with $2c/d \approx 1$ where it can be assumed the heat source passes through the middle of a cylindrical shell to solve the displacements ω and use the modified parameters β' and D'. Inertia friction welder for drill pipe and tube chassis construction are examples of possibles applications of further related research.

Bibliography

[1] C. Verhaeghe, *PREDICTIVE FORMULAE FOR WELDMENT DISTORTION - A CRITICAL REVIEW*. Cambridge CB1 6AH, England: Abington publishing, 1999.

[2] P. F. M. M. R. Grams, L. Ludwig, "A quantitative index to assess the influence of joint fit-up on pipeline weld root," *Proceedings of the ASME 2020*, 2020.

[3] T. L. E. COMPANY, *THE PROCEDURE HANDBOOK OF ARC WELDING*. 22801 St. Clair Avenue Cleveland, Ohio 44117: THE LINCOLN ELECTRIC COMPANY, 1973.

[4] D. Rosenthal, "The theory of moving sources of heat and its application to metal treatments," *Transactions of the A.S.M.E.*, 1946.

[5] Y. Lu, Y. Wang, and P. F. Mendez, "Width of thermal features induced by a 2-d moving heat source," *International Journal of Heat and Mass Transfer*, vol. 156, p. 119793, 2020.

[6] P. F. M. M. R. Grams, "A general expression for the tendon force in welding and additive manufacturing," *Journal of Manufacturing Science and Engineering*, 2020.

[7] A. F. T. I. F. S. VAIDYANATHAN, "Residual stresses due to circumferential welds," *Engineering Materials and Technology*, 1973.

[8] S. TIMOSHENKO, *THEORY OF PLATES AND SHELLS*. McGraw-Hill Book Company, Inc, 1959.

[9] R. Courant, *Calculus of Variations*. Courant Institute of Mathematical Sciences, 1963.

Annexes

A. Tendon force, thin plate constant properties

$$y_{max} = \sqrt{\frac{1}{2\pi e}}\left(\frac{Q'}{d\rho c}\right)\frac{1}{\Delta T_{max}}$$

$$(*)\Delta T_{max} = \sqrt{\frac{1}{2\pi e}}\left(\frac{Q'}{\rho c d}\right)\frac{1}{y_{max}}$$

$$\hat{F}_{ten} = -Ed\int_{y_{pl}} \varepsilon_{pl} dy$$

Applying symmetry and separating in regions II and III:

$$\hat{F}_{ten} = -2Ed[-\int_0^{y_{max}|_{T_{Y_2}}} \varepsilon_Y dy + \int_{y_{max}|_{T_{Y_2}}}^{y_{max}|_{T_{Y_1}}} \alpha(T_{Y_1} - T_{max})dy]$$

$$\hat{F}_{ten} = 2Ed[\int_0^{y_{max}|_{T_{Y_2}}} \varepsilon_Y dy + \int_{y_{max}|_{T_{Y_2}}}^{y_{max}|_{T_{Y_1}}} \alpha(T_0 + \Delta T_{max} - T_{Y_1})dy]$$

$$\hat{F}_{ten} = 2Ed[\varepsilon_Y y_{max}|_{T_{Y_2}} + \alpha\int_{y_{max}|_{T_{Y_2}}}^{y_{max}|_{T_{Y_1}}} T_0 dy - \alpha\int_{y_{max}|_{T_{Y_2}}}^{y_{max}|_{T_{Y_1}}} T_{Y_1} dy + \alpha\int_{y_{max}|_{T_{Y_2}}}^{y_{max}|_{T_{Y_1}}} \sqrt{\frac{1}{2\pi e}}\left(\frac{Q}{\rho c d}\right)\frac{1}{y_{max}} dy]$$

$$\hat{F}_{ten} = 2Ed[\varepsilon_Y y_{max}|_{T_{Y_2}} + \alpha T_0 y_{max}|_{T_{Y_2}}^{T_{Y_1}} - \alpha T_{Y_1} y_{max}|_{T_{Y_2}}^{T_{Y_1}} + \sqrt{\frac{1}{2\pi e}}(\frac{Q'}{\rho cd})\alpha \ln(y_{max})|_{T_{Y_2}}^{T_{Y_1}}]$$

$$(*)\ln(y_{max})|_{T_{Y_2}}^{T_{Y_1}} = \ln\left(\frac{y_{max}|_{T_{Y_1}}}{y_{max}|_{T_{Y_2}}}\right) = \ln\left(\frac{\Delta T_{Y_2}}{\Delta T_{Y_1}}\right) \approx \ln(2)$$

$$\hat{F}_{ten} = \frac{2EQ'}{\sqrt{2\pi e}\rho c}[\varepsilon_Y \frac{1}{\Delta T_{Y_2}} + (\alpha T_0 - \alpha T_{Y_1})(\frac{1}{\Delta T_{Y_1}} - \frac{1}{\Delta T_{Y_2}}) + \alpha \ln(2)]$$

$$\hat{F}_{ten} = \frac{2EQ'}{\sqrt{2\pi e}\rho c}[\varepsilon_Y \frac{1}{\Delta T_{Y_2}} - \alpha \Delta T_{Y_1}(\frac{\Delta T_{Y_2} - \Delta T_{Y_1}}{\Delta T_{Y_1}\Delta T_{Y_2}}) + \alpha \ln(2)]$$

$$\hat{F}_{ten} = \frac{2EQ'}{\sqrt{2\pi e}\rho c}[\varepsilon_Y \frac{1}{\Delta T_{Y_2}} - \overbrace{\alpha \frac{(T_{Y_2} - T_{Y_1})}{\Delta T_{Y_2}}}^{\varepsilon_Y} + \alpha \ln(2)]$$

$$\hat{F}_{ten} = \frac{2EQ'}{\sqrt{2\pi e}\rho c}\alpha \ln(2)$$

B. Strain Energy minimization

Follows minimize the function U:

$$U = \int_{-\infty}^{+\infty} \int_{-d/2}^{d/2} \frac{1}{2E} [\sigma_y^2 + \sigma_\theta^2 - 2\nu\sigma_y\sigma_\theta] dz dy$$

$$\sigma_\theta^2 = \sigma_H^2 + \frac{E^2\omega^2}{a^2} + \nu^2\sigma_y^2 + 2\left(\cancel{\nu\sigma_H\sigma_y} - \frac{E\sigma_H\omega}{a} - \cancel{\nu\frac{E\omega}{a}\sigma_y}\right)$$

$$\sigma_y^2 = \frac{E^2}{(1-\nu^2)^2}\omega''^2 z^2$$

$$2\nu\sigma_\theta\sigma_y = 2\nu\left(\cancel{\sigma_H\sigma_y} - \cancel{\frac{E\omega}{a}\sigma_y} + \nu\sigma_y^2\right)$$

$$\sigma_y^2 + \sigma_\theta^2 - 2\nu\sigma_\theta\sigma_y = \sigma_y^2 + \sigma_H^2 + \frac{E^2\omega^2}{a^2} - \nu^2\sigma_y^2 - 2\frac{E\sigma_H\omega}{a}$$

$$\sigma_y^2 + \sigma_\theta^2 - 2\nu\sigma_{theta}\sigma_y = \sigma_H^2 + \frac{E^2\omega^2}{a^2} + \cancel{(1-\nu^2)}\frac{E^2\omega''^2 z^2}{\cancel{(1-\nu^2)^2}} - 2\frac{\sigma_H E\omega}{a}$$

$$\int_{-\infty}^{+\infty} \int_{-d/2}^{d/2} \frac{1}{2E} [\sigma_y^2 + \sigma_\theta^2 - 2\nu\sigma_y\sigma_\theta] dz dy = \int_{-\infty}^{+\infty} \frac{d}{2E} [\sigma_H^2 + \frac{E^2\omega^2}{a^2} + \frac{E^2 d^2\omega''^2}{12(1-\nu^2)} - 2\frac{E\sigma_H\omega}{a}] dy$$

$$\int_{-\infty}^{+\infty} \left[\frac{d\sigma_H^2}{2E} + \frac{dE\omega^2}{2a^2} + \frac{D\omega''^2}{2} - \frac{d\sigma_H\omega}{a}\right] dy = \int_{-\infty}^{+\infty} F(y, \omega, \omega'') dy$$

$$F = \left[\frac{d\sigma_H^2}{2E} + \frac{dE\omega^2}{2a^2} + \frac{D\omega''^2}{2} - \frac{d\sigma_H \omega}{a} \right]$$

$$\frac{d^2}{dy^2}\left(\frac{\delta F}{\delta w''}\right) + \frac{\delta F}{\delta w} = 0 \Rightarrow \frac{d^2}{dy^2}\left(Dw''\right) + \frac{Ed}{a^2}w - \frac{d}{a}\sigma_H(y) = 0$$

$$\frac{d^2}{dy^2}\left(Dw''\right) + \frac{Ed}{a^2}w = \frac{d}{a}\sigma_H(y)$$

C. Strain Energy minimization from proposed stress field

Applying Hooke's law and adding σ_H to the angular component

$$\sigma_y = \frac{E}{1-\nu^2}(\varepsilon_y + \nu\varepsilon_\theta) = \frac{E}{1-\nu^2}\left(2zw'' - \nu\frac{w}{a}\right)$$

$$\sigma_\theta = \frac{E}{1-\nu^2}(\varepsilon_\theta + \nu\varepsilon_y) + \sigma_H = \frac{E}{1-\nu^2}\left(-\frac{w}{a} + 2\nu zw''\right) + \sigma_H$$

$$\sigma_y^2 = \left(\frac{E}{1-\nu^2}\right)^2\left(4z^2w''^2 + \nu^2\frac{w^2}{a^2} - \frac{4\nu w''z}{a}\right)$$

$$\sigma_\theta^2 = \left(\frac{E}{1-\nu^2}\right)^2\left(\frac{w^2}{a^2} + 4\nu^2w''^2z^2 - \frac{4\nu w''wz}{a}\right) + \sigma_H^2 + 2\sigma_H(\sigma_\theta - \sigma_H)$$

$$2\sigma_y\sigma_\theta = 2\left(\frac{E}{1-\nu^2}\right)^2\left(\nu\left[\frac{w^2}{a^2} + 4w''^2z^2\right] - 2(1+\nu^2)\frac{ww''z}{a}\right) + 2\sigma_H\sigma_y$$

Let be $\sigma_{\theta 1} = \sigma_\theta - \sigma_H$ and $\sigma^2 = \sigma_y^2 + \sigma_\theta^2 - 2\sigma_y\sigma_\theta$

$$\sigma^2 = \left(\frac{E}{1-\nu^2}\right)^2(1+\nu^2-2\nu)\left[4w''^2z^2 + \frac{w^2}{a^2} + 4\frac{w''wz}{a}\right] + \sigma_H^2 + 2\sigma_H\sigma_{\theta 1} - 2\sigma_H\sigma_y$$

$$\sigma^2 = \left(\frac{E}{1-\nu^2}\right)^2(1-\nu)^2\left[4w''^2z^2 + \frac{w^2}{a^2} + 4\frac{w''wz}{a}\right] + \sigma_H^2 + 2\sigma_H[\sigma_{\theta 1} - \sigma_y]$$

Let be $\alpha = \frac{(1-\nu)}{(1-\nu^2)}$

$$\sigma^2 = (E\alpha)^2 \left[4w''^2 z^2 + \frac{w^2}{a^2} + 4\frac{w''wz}{a}\right] + \sigma_H^2 + 2\sigma_H \left(\frac{E}{1-\nu^2}\right)(\nu-1)\left[2w''z + \frac{w}{a}\right]$$

$$\sigma^2 = (E\alpha)^2 \left[4w''^2 z^2 + \frac{w^2}{a^2} + 4\frac{w''wz}{a}\right] - 2\sigma_H(E\alpha)\left[2w''z + \frac{w}{a}\right] + \sigma_H^2$$

$$U = \int_{-\infty}^{+\infty} \int_{-d/2}^{d/2} \frac{1}{2E}[\sigma_y^2 + \sigma_\theta^2 - 2\nu\sigma_y\sigma_\theta]dzdy$$

Using symmetry on the z integration interval

$$U = \int_{-\infty}^{+\infty} \int_{-d/2}^{d/2} \frac{1}{2E}\left[(E\alpha)^2 \left[4w''^2 z^2 + \frac{w^2}{a^2} + 4\cancel{\frac{w''wz}{a}}\right] - 2\sigma_H(E\alpha)\left[\cancel{2w''z} + \frac{w}{a}\right] + \sigma_H^2\right] dzdy$$

$$\int_{-\infty}^{+\infty} \left[\frac{d\sigma_H^2}{2E} + \frac{4Ed^3w''^2\alpha^2}{24} + \frac{Ew^2d\alpha^2}{2a^2} - \frac{\sigma_H w d\alpha}{a}\right] dy = \int_{-\infty}^{+\infty} F(y, \omega, \omega'')dy$$

$$F = \left[\frac{d\sigma_H^2}{2E} + \frac{Ed^3w''^2\alpha^2}{6} + \frac{Ew^2d\alpha^2}{2a^2} - \frac{\sigma_H w d\alpha}{a}\right]$$

$$\frac{d^2}{dy^2}\left(\frac{\delta F}{\delta w''}\right) + \frac{\delta F}{\delta w} = 0 \Rightarrow \frac{d^2}{dy^2}(4D\alpha^2 w'') + \frac{Ed\alpha^2}{a^2}w = \frac{\alpha d}{a}\sigma_H(y)$$

$$\frac{d^2}{dy^2}\left(4Dw''\right) + \frac{Ed}{a^2}w = \frac{d}{a\alpha}\sigma_H(y)$$

If $\nu = 1/3 \Rightarrow \alpha \approx 0.77$

D. Script Rosenthal solutions calculator

```
close all
material = 'AISI 1018'; % Matereal selection(data from tello)
plate_type = 'thin'; % Plate geometry selection(thin or thick)
%Y= 6;%[mm]distance y from the moving source
q =6600;%[J/s] Amount of heat into the plate
U =    6.1; %[mm/s]
d = 0.011; %[m]
t_min = -5; %[seg]
t_max =20;% time frame afther the heat source pass
U = U*10^(-3);%[m/s];
Y=Y*10^(-3);%[m]
t=[t_min:0.1:t_max];
lapse=length(t);
Y=[0.003 0.004 0.006 0.012];

for i =[1:1:length(Y)]
    T=T_(t,plate_type,material,q,U,Y(i),d);
    plot(t,T, 'LineWidth',2)
    hold on
    grid on
end
legend('y = 3mm','y = 4mm','y = 6mm','y = 12mm')
plot([t_min,t_max],[293,293],'k-')
title(['Rosenthal solution T(t) ',plate_type,' ',material,' at distance y=',num2str(Y*10^3),'
    ↪ mm'])
xlabel('t')
ylabel('T[K]')
```

```
function T=T_(t,plate_type,material,q,U,y,d)
  T=zeros(1,length(t));
 [T_solidus,k,C_p,alpha,rho, nu] = ther_mec_parameters(material);%Thermal and
    ↪ mechanical_parameters
 %Table 3.1 from tello10_stwj_hot_deformation.
 switch plate_type
```

```
 case 'thick'
   z=0;
  for i = [1:1:length(t)]
   T(i)=T_thick(t(i),U,k,q,y,z,alpha);
  end
 case 'thin'
  h=1000;
  h1=h;
  h2=0;
  for i = [1:1:length(t)]
    T(i)=T_thin(t(i),U,k,q,y,h1,h2,d,alpha) ;
  end
 otherwise
   error('plot_hot_def - Fatal error! Illegal value of plate_type')
 end
end

```

```
% function T(t) Rosenthal thick 3d  :
function T = T_thick(t,U,k,q,y,z,alpha)
 xo= 0;
 To = 293 ;% kelvin
 x=xo-U*t;

 T=To + (q/(2*pi*k*sqrt(x^2+y^2+z^2)))*exp(-U*(x+sqrt(x^2+y^2+z^2))/(2*alpha));
 end

```

```
% function T(t) Rossenthal fiting thin plate or full penetration:
function T = T_thin(t,U,k,q,y,h1,h2,d,alpha)
 To = 293 ;%kelvin
 xo = 0; % in the meantime
 x = xo-U*t;
 T = To + (q/(2*pi*k*d))*exp(-U*x/(2*alpha))*besselk(0,(sqrt((U/(2*alpha))^2 + ((h1+h2)
    ↪ /(k*d)))*sqrt(x^2+y^2)));
 end

```

E. Numerical Results for Displacements

Table E.1: Numerically calculated radial displacements on the example

Radial displacement w[mm]	Position y[mm]
0,426	0
0,388	6,25
0,35	12,5
0,3097	18,7
0,27067	25
0,23467	31,2
0,20133	37,5
0,17267	43,7
0,148	50
0,0973	66,8
0,056	83,6
0,0273	98
0,00867	110
-0,00493	125
-0,01267	139
-0,01667	153
-0,018	165,5
-0,01706	182,3
-0,01467	200
-0,01067	220
-0,0073	245,3
-0,0037	274
-0,00106	302,5

Table E.2: Numerically calculated radial displacements case 1 at the weld trajectory ending

Radial displacement w[mm] x150	Position y[mm]
-76.7	0
-68.6	6
-61.4	12
-54.4	20
-47	25
-40.14	32
-33.8	38
-28.3	44.5
-23.4	50.5
-13.7	67
-6.3	83,7
1.3	98
1.7	110.5
3.8	125
5.1	139
5.6	153.5
5.6	166
5.2	183
4.7	200
3.8	221
2.95	246
2	274
1.37	302,5

F. Material characterization in numerical simulations

The material used in the numerical simulation is the *S*235 – *SPM_sw* of the library of Simufact welding created in JMatPro by J.Sakkiettibutra simulating the JIS SN400A steel.

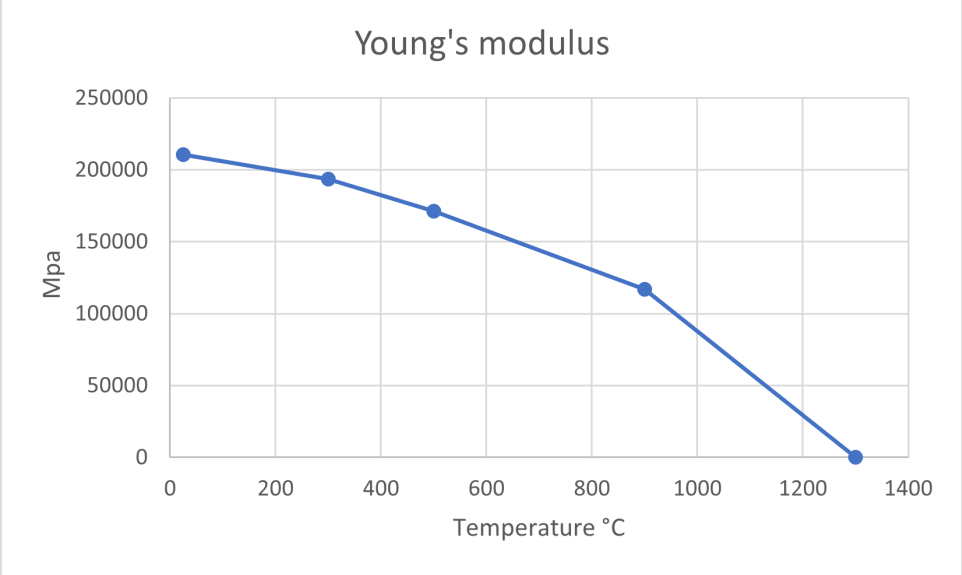

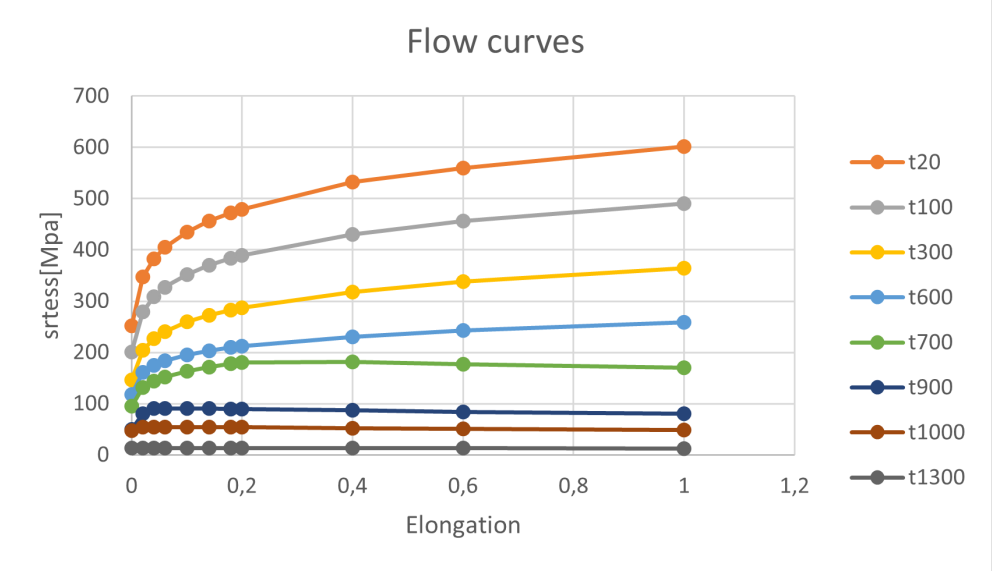

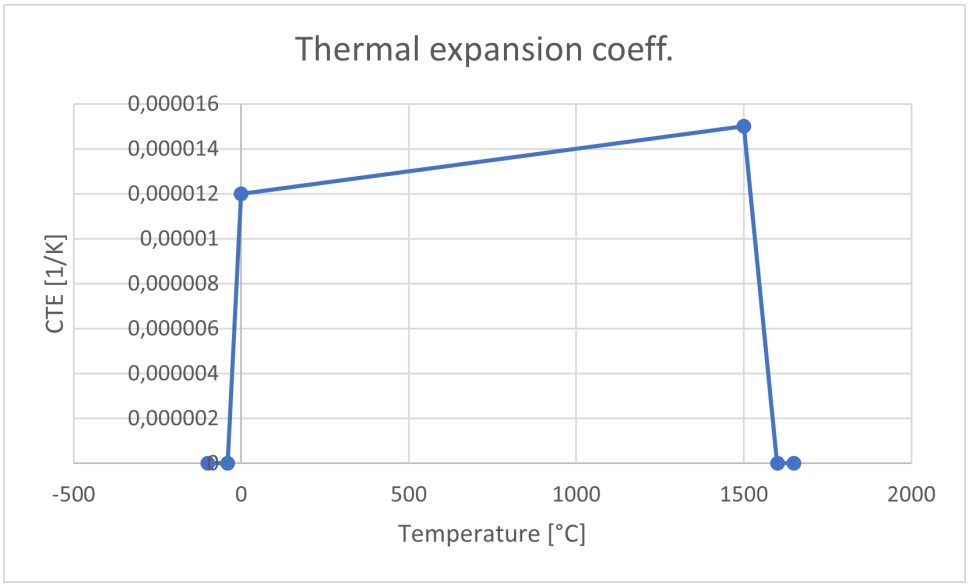
Thermal expansion coeff.
0,000016
0,000014
0,000012
0,00001
0,000008
0,000006
0,000004
0,000002
0
CTE [1/K]
-500
0
500
1000
1500
2000
Temperature [°C]

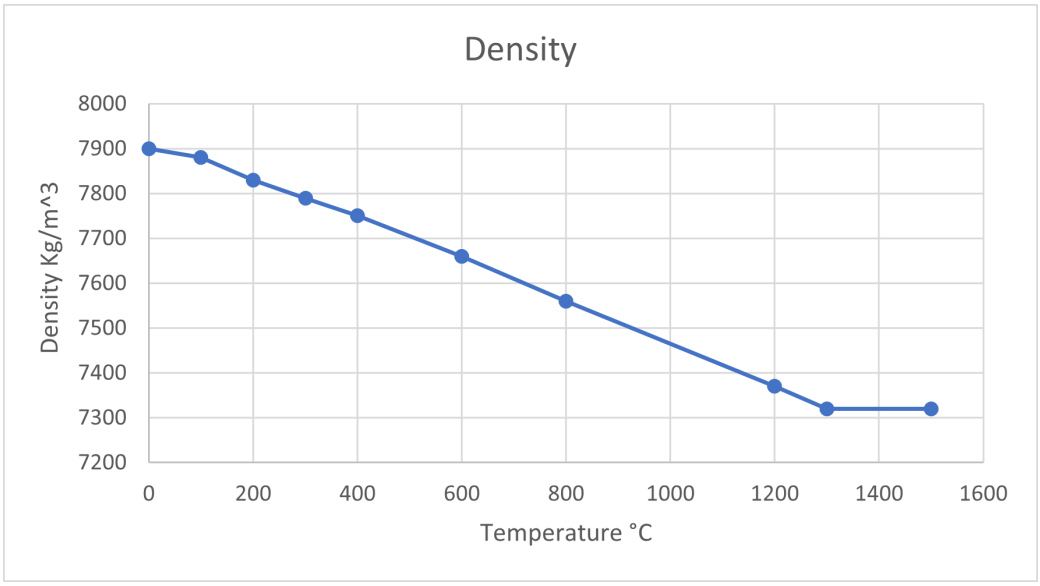
Density
8000
7900
7800
7700
7600
7500
7400
7300
7200
Density Kg/m^3
0
200
400
600
800
1000
1200
1400
1600
Temperature °C

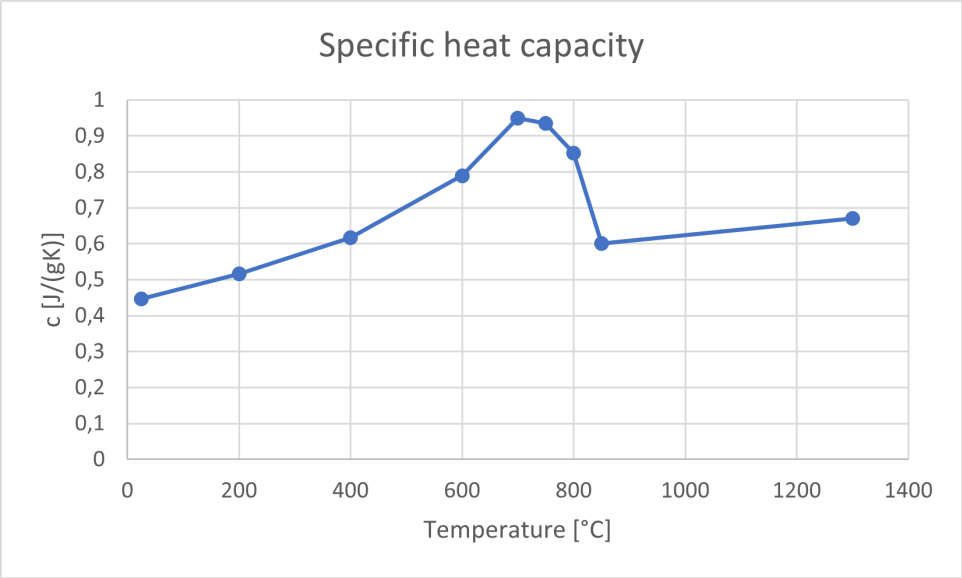
Specific heat capacity
c [J/(gK)]
1
0,9
0,8
0,7
0,6
0,5
0,4
0,3
0,2
0,1
0
0
200
400
600
800
1000
1200
1400
Temperature [°C]

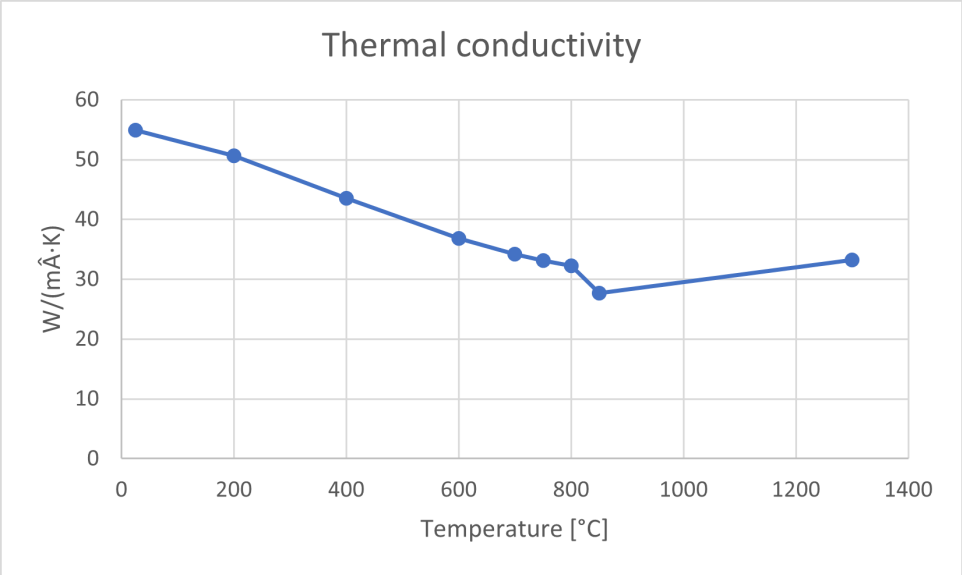
Thermal conductivity
W/(mÂ·K)
60
50
40
30
20
10
0
0
200
400
600
800
1000
1200
1400
Temperature [°C]